BOR DERGİSİ
JOURNAL OF BORON
https://dergipark.org.tr/boron

Selective lithium recovery from XRF melting waste via H_2TiO_3 ion sieve

Sezgin Özkasapoğlu [1,2,*], **Hüseyin Çelikkan** [1]

[1]Gazi University, Graduate School of Natural and Applied Sciences, Department of Chemistry, Ankara, Türkiye
[2]Turkish Energy, Nuclear and Mineral Research Agency, Boron Research Institute,Ankara, Türkiye
[3]Gazi University, Faculty of Sciences, Department of Chemistry, Ankara, Türkiye

ARTICLE INFO

Article History:
Received March 12, 2026
Accepted May 26, 2026
Available online June 30, 2026

Review Article

DOI: 10.30728/boron.1904399

Keywords:
Borate melting waste
Circular ecenomy
Lithium recovery
Titanium based ion-sieve

ABSTRACT

The growing demand for lithium driven by energy storage technologies requires sustainable recovery strategies from secondary resources. In this study, lithium recovery from lithium-rich X-Ray Fluorescence (XRF) melting waste was investigated using a titanium-based lithium-ion sieve via the ion-exchange method. Li_2TiO_3 (LTO) was synthesized by a solid-state method and converted into protonated H_2TiO_3 (HTO) through acid treatment to obtain a lithium-selective adsorbent. Structural and surface characterization confirmed the formation of a stable ion-sieve framework with increased surface area after proton exchange. XRF melting waste, mainly composed of lithium tetraborate and metaborate flux residues collected from cement plants, was subjected to acid digestion to selectively transfer lithium into the aqueous phase while minimizing co-dissolution of competing metals. Adsorption experiments revealed strong pH-dependent lithium uptake with a maximum capacity of ~36.0 mg g^{-1} under alkaline conditions. Isotherm and kinetic analyses indicated that the adsorption process follows the Langmuir model and pseudo-second-order kinetics, suggesting monolayer chemisorption governed by ion-exchange mechanisms. Thermodynamic evaluation showed that lithium adsorption was spontaneous and endothermic. The adsorbent exhibited high selectivity toward Li^+ in real waste-derived solutions and maintained stable performance over repeated adsorption-desorption cycles with minimal titanium leaching. This study demonstrates the feasibility of recovering lithium from XRF melting waste and highlights a new pathway for valorizing lithium and boron-rich residues within a circular economy framework.

1. Introduction

The rapid development of energy storage technologies, driven primarily by the widespread adoption of electric vehicles (EVs) and the integration of renewable energy sources, has led to a sharp increase in global lithium demand. Lithium is a critical raw material across a wide range of industrial sectors, and lithium compounds are extensively used in glass, ceramics, lubricating greases, and, most importantly, lithium-ion (Li-ion) batteries. In recent years, lithium consumption has increased significantly due to its intensive use in battery technologies, particularly in automotive applications [1]. The growing share of Li-ion batteries in the lithium market is largely attributed to the rapid global expansion of electric vehicle usage [2]. This pronounced upward trend is reflected in the dominance of the “Batteries” category among lithium end-use sectors, surpassing all other applications and emerging as the leading market segment [3].

In parallel, the greenhouse gas emissions resulting from fossil fuel consumption are among the primary drivers of global warming, positioning Li-ion batteries as a sustainable alternative to fossil-fuel-based energy systems. Interest in and demand for electric vehicles have increased rapidly in recent years, with global EV sales exceeding 17 million units in 2024. Projections indicate that this figure may surpass 20 million units in 2025, accounting for nearly one-quarter of total new vehicle sales worldwide (https://www.rsm.global/insights/2025-electric-vehicles-middle-market-outlook). Such rapid growth necessitates a substantial expansion in battery manufacturing capacity, thereby exerting strong upward pressure on lithium demand.

The escalating demand has placed significant stress on lithium supply chains, prompting many countries to accelerate investments in lithium exploration, mining, and processing technologies [4]. In recent years, a notable shift has occurred in the global lithium supply structure [5]. While brine resources in South America historically dominated global lithium production, hard-rock spodumene production in Australia has rapidly expanded and now accounts for more than half of the world’s primary lithium supply [6]. Lithium resources occur in two primary forms: hard-rock mineral deposits such as spodumene and lepidolite, and liquid-phase brine resources including salt lake brines, geothermal brines, and oilfield waters, with brine sources accounting for approximately 64% of total global lithium reserves [7].

*Corresponding author: sezgin.ozkasapoglu@gazi.edu.tr

© 2026 Turkish Energy Nuclear and Mineral Research Agency
CC BY-NC-SA 4.0

The rapid growth in global demand clearly indicates that primary lithium resources alone may not be sufficient to ensure long-term supply security [3]. Consequently, secondary lithium resources-particularly industrial process waste, metallurgical residues, and spent Li-ion batteries-are gaining strategic importance for establishing a sustainable lithium supply [8]. In this context, increasing attention has been directed toward lithium recovery from waste materials to reduce dependence on conventional resources, lower costs, and minimize environmental impacts [9].

Lithium can be recovered from primary and secondary resources using several technological routes. Pyrometallurgical methods typically involve high-temperature treatment of lithium-bearing minerals to concentrate lithium phases, whereas hydrometallurgical approaches rely on leaching followed by purification steps such as precipitation, solvent extraction, or ion Exchange [10]. Among the methods developed for aqueous lithium extraction, chemical precipitation offers operational simplicity and low cost but is primarily applicable to brines with low Mg/Li ratios and suffers from low recovery rates and time-consuming processing [10, 11]. Solvent extraction, employing organic extractants such as tributyl phosphate (TBP) or ionic liquid systems, demonstrates high efficiency for high Mg/Li ratio brines but is hampered by complex solvent preparation, high operational costs, and difficulties in extractant recovery [12, 13]. Membrane-based separation technologies - including nanofiltration (NF), reverse osmosis (RO), selective electrodialysis (S-ED), and bipolar membrane electrodialysis (BMED) - offer high recovery rates and are suitable for brines with high Mg/Li ratios; however, membrane fouling, high capital costs, and sensitivity to brine composition remain significant challenges [14-17]. Electrochemical methods, such as capacitive deionization (CDI), electrochemically switched ion exchange (ESIX), and electrochemical lithium-ion pumping (ELIP), are capable of processing both high and low Mg/Li ratio brines with high selectivity, although they require substantial energy input and precise electrolyte management [18, 19]. To overcome the inherent limitations of individual technologies, coupled and tandem approaches - including the integration of adsorption with electrochemical processes, membrane distillation with crystallization, and multistage selective electrodialysis - have been increasingly explored and demonstrated the potential to simultaneously improve separation efficiency and extraction capacity while reducing energy consumption [7, 20, 21]. Furthermore, some of these integrated systems, such as membrane distillation-crystallization (MDC), offer the dual benefit of efficient lithium concentration and simultaneous fresh water recovery, thereby paving the way for sustainable zero-liquid discharge (ZLD) frameworks [22].

Among theses technologies, adsorption-based methods-along with electrochemical and membrane-assisted processes-have attracted considerable attention due to their high selectivity, operational flexibility, and suitability for treating dilute and chemically complex aqueous systems.[15, 23, 24]. A growing number of studies have demonstrated the feasibility of recovering lithium from diverse aqueous sources beyond conventional salt lake brines [25, 26]. Electrochemical intercalation/de-intercalation using $LiFePO_4/FePO_4$ electrodes has been reported as a promising approach for lithium recovery from high Mg/Li ratio brines [27, 28]. Ion exchange combined with ultrafiltration membrane filtration has also been successfully applied for the separation of lithium from geothermal water using λ-MnO_2 adsorbent, with optimal operating conditions yielding complete lithium removal [29]. Ion exchange resins have been employed for selective lithium recovery from geothermal brines, with Lewatit TP 260 resin achieving a maximum Li recovery rate of 71% from geothermal waters in Türkiye [30]. Similarly, chitosan-coated lithium manganese oxide composites (CTS/LMO) have been applied to geothermal brines from Germencik and Tuzla in Türkiye, yielding maximum adsorption capacities of approximately 3.6 mg g^{-1} [31]. In particular, adsorption-based approaches have gained prominence among these technologies due to their inherent selectivity and adaptability to complex aqueous systems, making them especially suitable for lithium recovery from dilute and multi-component matrices [24, 32]. Within adsorption-based systems, lithium-ion sieve (LIS) materials have been extensively investigated, particularly manganese-based (LMO) and titanium-based (LTO) adsorbents [33]. LMO-type materials generally exhibit high adsorption capacities due to their favorable spinel structure; however, they often suffer from manganese dissolution and structural degradation, especially under acidic desorption conditions [34, 35]. In contrast, titanium-based ion sieves, such as H_2TiO_3 (HTO), offer superior chemical stability owing to the strong Ti-O framework, resulting in lower dissolution loss and improved cyclic stability [15, 36]. herefore, titanium-based ion-sieve adsorbents are considered promising candidates for sustainable and selective lithium recovery [37]. Recent studies have explored titanium-based lithium-ion sieve materials in advanced configurations, such as 3D-printed monolithic structures, demonstrating improved mechanical strength and promising adsorption performance for lithium recovery from aqueous systems [38]. Moreover, heteroatom doping strategies, such as Co and N co-doping in HTO structures, have been reported to enhance lithium adsorption capacity and kinetics by increasing active sites and promoting ion diffusion through the formation of oxygen vacancies [39]. Similarly, synergistic surface coating and elemental doping strategies have been explored to simultaneously enhance adsorption capacity and structural stability of manganese-based ion-sieves. Zhang et al. demonstrated that converting lithium residues on $Li_{1.6}Mn_{1.6}O_4$ surfaces into lithium lanthanum titanate (LLTO) through combined La and Ti incorporation resulted in a notable increase

in adsorption capacity from 31.81 to 35.66 mg g^{-1}, alongside a reduction in manganese dissolution rate from 2.54% to 1.93%. DFT calculations confirmed that the synergistic effects of surface coating and gradient doping lowered the Li^+ migration energy barrier from 2.70 to 0.41 eV, thereby facilitating ion transport and suppressing undesirable side reactions [40].

Although titanium-based ion-sieve adsorbents have been previously investigated for lithium recovery, their application to lithium recovery from XRF melting waste has not yet been reported. By valorizing this underutilized analytical waste as a potential unconventional secondary lithium resource, the present study not only introduces a pioneering application but also contributes to circular economy principles and waste minimization, thereby clearly demonstrating its originality and scientific novelty.

In this context, particular attention has been given to lithium tetraborate/metaborate melting samples used in XRF analysis, which are classified as waste after use. Owing to their relatively high lithium content (~8.5 wt%), these materials constitute a representative example of lithium-bearing industrial waste that can serve as a case study for evaluating the feasibility of lithium recovery from unconventional secondary sources. In Türkiye alone, the approximately 5 tons of such waste generated annually underscores the existence of largely overlooked lithium-containing residues in industrial processes, and highlights the importance of developing recovery methodologies applicable to similar waste streams within a circular economy framework.

This study aims to investigate lithium recovery from XRF melting waste as a case study, focusing on the feasibility of utilizing a lithium-containing analytical residue. Within this scope, XRF melting waste collected from cement plants was treated using a titanium-based lithium-ion sieve as a lithium-selective adsorbent. The recovery performance was evaluated under various operational conditions, and adsorption behavior was analyzed to assess the applicability of the system. Furthermore, selectivity and desorption-regeneration characteristics were investigated to determine the practical usability and sustainability of the adsorbent.

2. Experimental

2.1. Reagents

Lithium carbonate (Li_2CO_3, >99%, Merck, Germany) and titanium dioxide (TiO_2, 99.9%, Aladdin, China) were used for Li_2TiO_3 synthesis. Lithium chloride (LiCl, 99.9%, Aladdin, China) was used to prepare aqueous lithium solutions. Hydrochloric acid (HCl, 37%, Merck, Germany) was used for elution, sodium hydroxide (NaOH, Merck, Germany) for pH adjustment, and sulfuric acid (H_2SO_4, 98%, Merck, Germany) for digestion of XRF waste. All solutions were prepared using ultrapure water (18.2 MΩ·cm). All chemicals were analytical grade and used without further purification.

2.2. Preparation of LTO and HTO

LTO was synthesized via solid-state reaction using stoichiometric amounts of Li_2CO_3 and TiO_2 dispersed in 50 mL anhydrous ethanol, following a modified procedure based on Zhang et al [41]. The overall synthesis procedure is schematically illustrated in Figure 1.

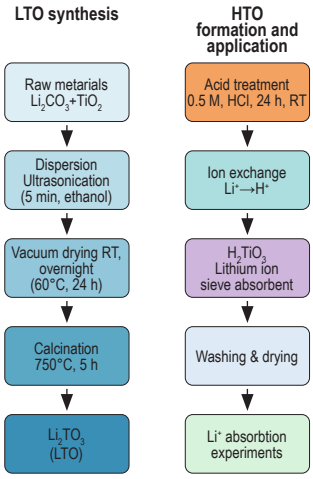


Figure 1. Schematic illustration of the synthesis of LTO and its formation into HTO, followed by adsorption experiments. RT denotes room temperature.

As shown in Figure 1, the suspension was sonicated for 5 min to ensure homogeneous mixing, then dried at room temperature overnight and further dehydrated in a vacuum oven at 60°C for 24 h. The resulting powder was calcined at 750°C for 5 h to obtain the LTO crystalline phase. To produce the ion-sieve adsorbent (HTO), the calcined LTO was treated with 0.5 M HCl at room temperature for 24 h under constant stirring, facilitating partial extraction of Li^+ from the crystal lattice and yielding the protonated H_2TiO_3 structure used in subsequent adsorption experiments.

2.3. Acid Digestion of Melting Sample

Approximately 42 kg of smelting residue was crushed and ground to obtain a representative powder (~100 µm). Acid leaching was performed using 1.0 M H_2SO_4 in a 150 mL Teflon-lined stainless steel autoclave at 200°C for 2 h to enhance lithium dissolution under elevated temperature and pressure conditions. After cooling to room temperature, the slurry was filtered using 0.22 µm syringe filters, and the filtrate was collected for subsequent adsorption experiments. Filtration was carried out in multiple batches to ensure complete solid-liquid separation.

2.4. Characterization

A systematic characterization approach was adopted to elucidate the structural, compositional, and surface-related properties of the synthesized lithium

titanate-based adsorbents. Phase identification, crystallographic structure, and crystallinity were examined by X-ray diffraction (XRD, PANalytical/ Empyrean, Netherlands) to verify the formation of the desired Li_2TiO_3 phase and confirm the completion of the solid-state synthesis.

For the solid waste materials, the overall chemical composition was first determined by X-ray fluorescence spectroscopy (XRF, PANalytical/ Epsilon1, Netherlands) to determine the major oxide composition. After acid digestion and pH adjustment of the waste samples, the elemental concentrations in the resulting leachates were quantified by inductively coupled plasma optical emission spectrometry (ICP-OES, Thermo Scientific/ICAP7000, USA) to determine lithium and coexisting metal ions, and the same technique was used to monitor lithium concentrations in the adsorption experiments.

The morphological features and surface texture of the adsorbent were investigated using scanning electron microscopy (SEM, Hitachi/SU5000, Japan).

Surface chemical composition and oxidation states were examined by X-ray photoelectron spectroscopy (XPS, Thermo Scientific/K-Alpha, USA), enabling detailed analysis of surface elemental distribution, chemical states, and adsorption-active sites associated with lithium uptake. The specific surface area of the adsorbent was determined by N_2 adsorption using the Brunauer-Emmett-Teller (BET, Anton Paar/Autosorb, Austria) analysis to assess pore accessibility and adsorption site availability. Zeta potential measurements were performed using a Zetasizer (Malvern/Nano ZSP, UK) instrument to evaluate the surface charge characteristics of the adsorbents.

In addition, the wettability of the adsorbent was evaluated by static water contact angle measurements using a KSV CAM 200 optical goniometer (KSV Instruments, Helsinki, Finland) to assess its hydrophilic or hydrophobic surface characteristics and their influence on adsorption and elution performance. Fourier transform infrared spectroscopy (JASCO/FT-IR6X, Tokyo, Japan) was employed to identify functional groups, metal-oxygen bonding environments, and structural changes occurring before and after adsorption and elution processes, thereby providing insight into the mechanisms governing lithium adsorption.

2.5. Adsorption and Desorption Experiments

2.5.1. Influence of pH on lithium adsorption

The effect of solution pH on lithium adsorption was investigated using batch experiments. Lithium solutions (≈200 mg L^{-1}, 100 mL) were adjusted to pH values between 4 and 11 using 1 M NaOH and HCl prior to adsorbent addition. The suspensions were stirred at 200 rpm at ambient temperature for 24 h to ensure equilibrium. After separation of the solid phase, the residual lithium concentration in the supernatant was determined by ICP-OES. The equilibrium adsorption capacity (q_e, mg g^{-1}) was calculated using the following equation:

$$q_e = \frac{(C_0 - C_e) \times V}{m} \quad (1)$$

In this equation, C_0 (mg L^{-1}) represents the initial lithium concentration, while C_e (mg L^{-1}) denotes the lithium concentration at equilibrium. V (L) corresponds to the volume of the aqueous phase, and m (g) refers to the amount of adsorbent employed during the adsorption experiment.

2.5.2. Effect of solid-to-liquid (S/L) ratio on lithium adsorption

The effect of the solid-to-liquid (S/L) ratio on lithium adsorption was investigated by varying the adsorbent dosage from 1 to 10 g L^{-1}. The experiments were conducted by adding a known amount of HTO adsorbent into lithium-containing solutions of fixed initial concentration under constant pH and temperature conditions. The suspensions were agitated for 24 h to ensure equilibrium was reached. After adsorption, the solid and liquid phases were separated by centrifugation, and the residual lithium concentration in the solution was analyzed to determine the adsorption performance at different S/L ratios.

2.5.3. Adsorption isotherms

Adsorption isotherm studies were conducted using HTO at a fixed dosage of 1 g L^{-1}. Batch experiments were performed at room temperature with initial lithium concentrations ranging from 25 to 200 mg L^{-1} (100 mL), and the suspensions were stirred at 200 rpm for 24 h to ensure equilibrium. After phase separation, the lithium concentration in the supernatant was determined by ICP-OES. The equilibrium adsorption capacity was calculated using equation (1), and the data were analyzed using Langmuir and Freundlich isotherm models.

2.5.4. Adsorption thermodynamics

Thermodynamic studies were conducted to evaluate the effect of temperature on lithium adsorption. Batch experiments were performed at 298, 308, and 318 K using lithium solutions (25-200 mg L^{-1}, 100 mL) at a fixed pH of 12, selected based on preliminary experiments indicating optimal adsorption under alkaline conditions. The suspensions were stirred at 200 rpm for 24 h to ensure equilibrium. After phase separation, lithium concentrations in the supernatant were determined by ICP-OES. Adsorption isotherms were obtained at each temperature and analyzed using Langmuir and Freundlich models. Thermodynamic parameters ($\Delta G°$, $\Delta H°$, $\Delta S°$) were calculated from the Langmuir equilibrium constants using the following equations [42]:

$$\Delta G^0 = -RT\ln K^0 \quad (2)$$

$$\ln K^0 = -\frac{\Delta H^0}{RT} + \frac{\Delta S^0}{R} \quad (3)$$

Here, *R* denotes the universal gas constant (8.314 J·mol^{-1}·K^{-1}), *T* corresponds to the absolute temperature in Kelvin, and *K* refers to the equilibrium constant of the adsorption process. The thermodynamic parameters ΔH° and ΔS° were determined from the slope and intercept, respectively, of the linear plot obtained by graphing lnK_0 against *1/T*.

2.5.5. Adsorption kinetics

Adsorption kinetic studies were conducted at 308 K to investigate lithium uptake rate and mechanism. Batch experiments were performed using 100 mL of lithium solution (≈200 mg·L^{-1}), and aliquots (100 µL) were withdrawn at predetermined time intervals over 24 h. After centrifugation, the supernatant was analyzed by ICP-OES. The adsorption capacity at each time was calculated using Equation 1. All experiments were carried out under previously optimized conditions.

2.5.6. Recycling experiments

The adsorption-desorption behavior and reusability of HTO were evaluated through successive batch cycles. In each cycle, 100 mL of lithium solution (≈200 mg L^{-1}) was contacted with the adsorbent at a solid-to-liquid ratio of 1 g·L^{-1} under fixed conditions (pH 12, 308 K, 6 h). After adsorption, the phases were separated and the solution was analyzed for lithium concentration. The adsorbent was regenerated using 0.5 M HCl for 4 h, as commonly reported for efficient Li^+ desorption from titanium-based ion-sieve materials [43]. The concentrations of lithium and titanium released into the eluent were determined by ICP-OES. The regenerated adsorbent was subsequently washed with deionized water to neutral pH, dried, and reused in subsequent cycles. This procedure enabled the evaluation of adsorption capacity retention and long-term stability.

2.5.7. Adsorption and selectivity behavior of HTO in real waste-derived solutions

The lithium selectivity of the adsorbent was investigated using a real leachate obtained from the dissolution of solid XRF melting waste, in which lithium was released into the aqueous phase along with various coexisting impurity ions. In these experiments, approximately 0.1 g of the adsorbent was introduced into the solution containing lithium and representative competing metal ions commonly associated with XRF melting waste, such as Na^+, Mg^{2+}, B^{3+}, Si^{4+}, Ca^{2+}, K^+, and Fe^{3+}. Batch adsorption tests were then performed under a constant temperature of 308 K. Following the completion of the adsorption process, solid-liquid separation was carried out, and the remaining concentrations of lithium and competing ions in the solution were determined. The selectivity performance of the adsorbent was evaluated by calculating selectivity-related parameters using the Equation 3, 4 presented below, enabling a quantitative assessment of lithium's preferential adsorption behavior in the presence of competing species [44].

$$K_d = \frac{(C_0 - C_e)}{m \times C_e} \times V \quad (4)$$

$$\alpha_M^{Li} = \frac{K_{d(Li)}}{K_{d(M)}} \quad (5)$$

Where K_d (mLg^{-1}) is the distribution coefficient reflecting the adsorption affinity of the adsorbent toward a given ion, α_M^{Li} is the selectivity coefficient describing the preferential adsorption of lithium ions over a competing metal ion (M).

2.5.8. Desorption experiments in real sample

Desorption experiments were conducted to evaluate the regeneration efficiency and selectivity of the lithium-loaded HTO adsorbent in the presence of competing ions. After the adsorption step, the solid phase contacted with 100 mL of 0.5 M HCl solution under continuous stirring (200 rpm) at room temperature for 4 h. Following desorption, the suspension was separated by centrifugation, and the concentrations of lithium and co-existing metal ions in the supernatant were determined using ICP-OES. The desorption efficiency (%) for each ion was calculated based on the ratio of the amount released during desorption to the amount previously adsorbed. The regenerated adsorbent was subsequently washed with deionized water until neutral pH, dried, and reused in subsequent cycles.

3. Results and Discussion

3.1. Material Characterization

XRD patterns of LTO and protonated HTO are presented in Figure 2.

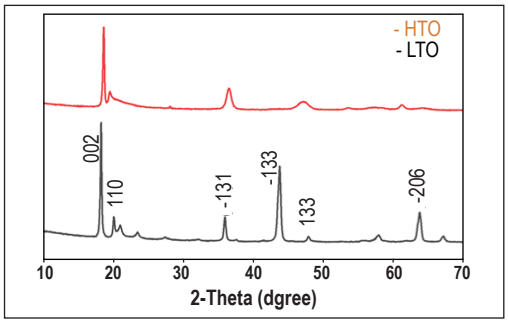


Figure 2. XRD patterns of LTO and protonated HTO.

The diffraction peaks of LTO match well with the standard monoclinic Li_2TiO_3 phase (ICSD PDF No. 98-016-2215), confirming the successful formation of a single-phase LTO structure [44]. The characteristic reflections indexed to the (002), (110), (-131), (-133), (133), and (-206) planes confirm the formation of a well-crystallized LTO phase (Figure 2) [45, 46]. Following proton exchange, the HTO sample exhibits

a noticeable decrease in peak intensity and peak broadening, indicating a partial loss of crystallinity. This behavior is commonly attributed to structural distortion and defect formation induced by Li^+/H^+ ion exchange, where the removal of lithium from the lattice generates vacancies and disrupts long-range order [44, 47]. In addition, a slight shift of the diffraction peaks toward higher 2θ values is observed, suggesting lattice contraction. This can be explained by the substitution of Li^+ ions (ionic radius ≈0.76 Å) with significantly smaller H^+ ions, leading to a reduction in lattice parameters. Similar peak shifts have been widely reported for protonated titanium-based ion sieves and are considered a characteristic indicator of successful Li^+ extraction and proton insertion into the host structure [47, 48]. Despite these structural modifications, no new diffraction peaks are detected, and the overall diffraction pattern remains consistent with that of the parent LTO phase. This indicates that the fundamental layered framework is preserved during protonation, which is a critical requirement for maintaining structural integrity and adsorption performance [49, 50]. Such structural stability has been reported as a key advantage of titanium-based ion sieves compared to manganese-based analogues, which often suffer from framework degradation during acid treatment [44, 51]. The preservation of the host lattice, combined with the formation of lithium vacancies, plays a crucial role in enabling selective lithium adsorption. These vacancies act as specific binding sites for Li^+ ions during subsequent adsorption cycles, thereby contributing to the ion-sieving mechanism and ensuring high selectivity and cyclic stability of HTO [32].

In addition to the structural analysis, the textural properties of the HTO were evaluated by Brunauer-Emmett-Teller (BET) surface area analysis. The pristine LTO exhibited a specific surface area of 8.2 $m^2 \cdot g^{-1}$, whereas the proton-exchanged HTO showed a significantly higher value of 18.6 $m^2 \cdot g^{-1}$, indicating that acid treatment effectively enhances the accessible surface area. This increase can be attributed to partial lithium removal and structural rearrangement during the Li^+/H^+ exchange process, which promotes the formation of additional surface accessibility without destroying the bulk framework [34]. The obtained surface area of HTO is notably higher than those typically reported for solid-state synthesized HTO (ranging from ~4 to 6 $m^2 \cdot g^{-1}$) [52], yet consistent with modified or optimized solid-state precursors (14-28 $m^2 \cdot g^{-1}$) described in recent studies [53]. This surface area corresponds well with the dense and well-crystallized nature of HTO observed in the XRD results, where sharp diffraction peaks reflect limited structural disorder and relatively compact particle packing [54]. Although the surface area is not exceptionally high compared to hydrothermally synthesized porous nanomaterials [55, 56], it is sufficient to provide accessible active sites for lithium adsorption, particularly when combined with the intrinsic lithium-memory effect of the titanate framework [57]. Moreover, this moderate BET surface area suggests a favorable balance between structural stability and adsorption accessibility, which is essential for minimizing titanium dissolution and maintaining ion-sieve integrity during repeated adsorption-desorption cycles [58]. The surface wettability of the HTO adsorbent was evaluated by static water contact angle measurements (Figure 3).

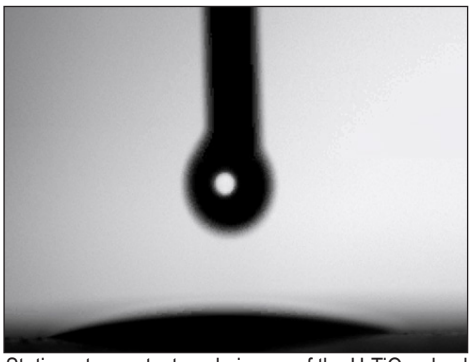


Figure 3. Static water contact angle image of the H_2TiO_3 adsorbent.

The measurement was performed on a pelletized form of the powder adsorbent to provide qualitative insight into its surface wettability. The measured contact angle of 28.7° indicates a highly hydrophilic surface. Although a specific 'ideal' contact angle value is not defined for lithium-ion sieve adsorbents, hydrophilic surfaces (contact angle < 90°) are generally considered favorable, as they enhance electrolyte spreading and facilitate Li^+ transport to active sites [42, 56]. It should be noted that, for powder-based materials, contact angle values are considered semi-quantitative and are primarily used for comparative assessment rather than absolute evaluation. Nevertheless, the low contact angle suggests favorable wettability, which can facilitate electrolyte spreading and enhance Li^+ transport toward adsorption sites [56].

The SEM micrographs shown in Figure 4 reveal that acid elution does not induce a significant morphological transformation in the material. As observed by comparing Figure 4a (LTO) and Figure 4b (HTO), both samples display a similarly compact morphology composed of agglomerated secondary particles with densely packed primary grains, and the overall particle shape, size distribution, and surface texture are largely preserved following acid treatment. This observation is consistent with findings reported in the literature, where the acid pickling process has been shown to exert little effect on the particle morphologies and sizes of LTO-derived adsorbents [44, 59], confirming that the structural integrity of the material is maintained during delithiation.

The retention of morphology upon acid elution, however, does not imply that the material undergoes no meaningful transformation. Rather, the changes induced by acid treatment are primarily chemical and crystallographic in nature, occurring at a scale below

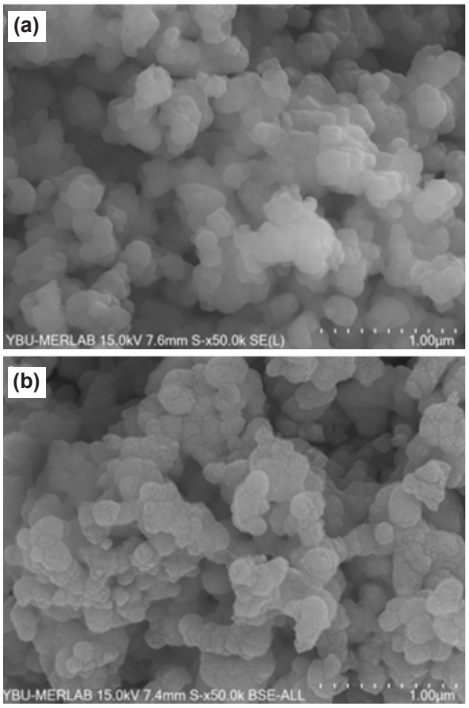


Figure 4. SEM images of (a) LTO and (b) HTO.

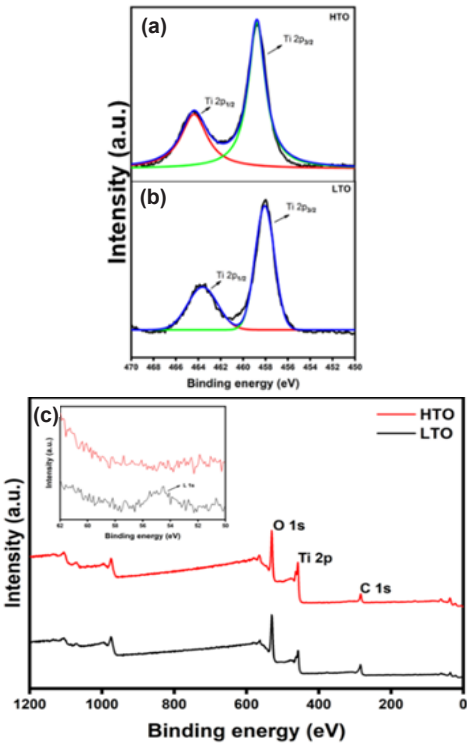


Figure 5. XPS spectra of LTO and HTO: (a) high-resolution Ti 2p spectrum of HTO, (b) Ti 2p spectrum of LTO, and (c) survey spectra of both samples. The inset in (c) shows the Li 1s region, indicating lithium removal after acid treatment.

the resolution of SEM imaging. The replacement of Li^+ by H^+ within the layered framework results in modifications to the interlayer spacing and local bonding environment, as evidenced by the XRD and FTIR results discussed elsewhere in this work. XPS analysis of acid-treated HTO confirms the disappearance of the Li 1s signal and the transformation from Li-O to H-O bonding after acid treatment [60], demonstrating that substantial chemical restructuring occurs at the atomic level despite the macroscopic morphological similarity observed in SEM.

The functional implications of this chemical transformation are further reflected in the BET surface area results. Although the SEM images do not reveal a pronounced difference in particle architecture between LTO and HTO, the BET analysis indicates an increase in accessible surface area following acid elution. This improvement is attributed not to large-scale morphological reorganization, but to the opening of previously blocked micropores and the increased surface hydroxyl group density resulting from H^+ incorporation. It has been established that the practical Li^+ adsorption capacity of HTO is closely linked to its specific surface area, as a larger contact area exposes more active ion-exchange sites and facilitates Li^+ diffusion toward the interior of the adsorbent particles [56, 61]. Accordingly, the improvement in textural properties measured by BET, rather than any gross morphological change visible in SEM, is the principal factor governing the enhanced adsorption performance of HTO relative to its LTO precursor.

The XPS spectra of LTO and HTO are presented in Figure 5. The survey spectra (Figure 5c) confirm the presence of Ti and O as the dominant elements, while the Li 1s signal is significantly suppressed after acid treatment, indicating effective lithium extraction. This decrease in Li content is associated with the formation of lithium vacancies within the lattice, which are known to act as active sites for subsequent Li^+ adsorption in ion-sieve materials [32, 62]. The high-resolution Ti 2p spectra of LTO and HTO (Figure 5a and 5b) display well-defined Ti $2p_{3/2}$ and Ti $2p_{1/2}$ peaks centered at ~458.5 eV and ~464.2 eV, with a spin-orbit splitting of approximately 5.6-5.7 eV. These values are characteristic of Ti^{4+} species, confirming that the oxidation state of titanium remains unchanged after acid treatment. The absence of any Ti^{3+} contribution indicates that the Ti-O framework remains chemically stable and that no reduction process occurs during lithium extraction [56, 60, 63]. This behavior suggests that the lithium removal process proceeds predominantly via a Li^+/H^+ ion-exchange mechanism rather than a redox reaction, which is consistent with previous studies on titanium-based ion-sieve materials [56, 63]. In contrast to manganese-based adsorbents, where partial reduction and structural degradation are often observed, the preservation of Ti^{4+} highlights the superior chemical stability of HTO under acidic conditions [34, 64]. Furthermore, the generation of lithium vacancies, together with the maintained Ti-O framework, plays a critical role in enabling selective lithium adsorption. These vacancies act as specific binding sites for Li^+ ions during adsorption, supporting the ion-sieving mechanism and contributing to the high selectivity and cyclic stability observed for HTO [32, 62].

As shown in Figure 6, the FTIR spectra of LTO and HTO exhibit characteristic vibrational bands associated with the titanate framework and surface hydroxyl groups [34]. The broad absorption band in the 3200-3500 cm^{-1} region, assigned to *ν*(O-H) stretching vibrations, becomes significantly broader and more intense in the HTO spectrum. This indicates the formation of additional hydroxyl groups as a result of Li^+/H^+ ion exchange, which introduces protonated sites within the structure [44, 65]. Such hydroxyl enrichment is widely reported for protonated titanate materials and is considered a key feature contributing to their ion-exchange capability. The band at ~1630 cm^{-1} corresponds to δ(H-O-H) bending vibrations of adsorbed water molecules, and its increased intensity in HTO suggests enhanced surface hydration, which can facilitate Li^+ diffusion during adsorption [44, 66].

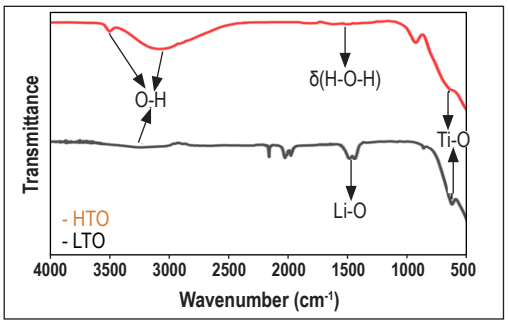


Figure 6. FT-IR spectra of LTO and HTO.

In the lower wavenumber region (600-700 cm^{-1}), the strong bands assigned to Ti-O and Ti-O-Ti lattice vibrations are observed in both LTO and HTO, confirming that the fundamental titanate framework remains intact after acid treatment [59, 60]. This structural preservation is consistent with previous studies on titanium-based ion sieves and is essential for maintaining adsorption stability during repeated cycles.

Notably, the Li-O vibration band observed at ~1400-1500 cm^{-1} in LTO significantly decreases or disappears after acid treatment, providing clear evidence of lithium extraction [44, 67]. This removal of Li^+ ions leads to the formation of vacant sites within the lattice, which serve as selective adsorption sites for lithium ions during subsequent adsorption processes [32, 62].

Overall, the FTIR results confirm that the acid treatment induces protonation and lithium removal while preserving the titanate framework [47, 56]. The combination of newly formed hydroxyl groups and lithium vacancies plays a crucial role in the ion-sieving mechanism, enhancing both the selectivity and adsorption performance of HTO [57, 68].

3.2. Selective Lithium Dissolution from XRF Melting Waste: Effect of Acid Digestion and pH Adjustment on Solution Chemistry

As summarized in Table 1, the melting solid sample exhibits a boron-rich composition, dominated by B_2O_3 (59.4 wt%) and containing a significant amount of Li_2O (18.4 wt%). CaO (12.79 wt%) and SiO_2 (4.49 wt%) are present as secondary components, while Na_2O, K_2O, Fe_2O_3, and MgO occur only in minor quantities. This compositional profile indicates that the waste is not only rich in lithium but also contains a relatively simple impurity matrix, which is advantageous for selective lithium extraction. Furthermore, the high initial lithium content provides a suitable basis for evaluating dissolution efficiency and lithium transfer into the aqueous phase during the subsequent digestion process.

Table 1. Chemical composition of XRF melting waste and solution chemistry after dissolution and pH adjustment

Component	Solid waste (wt%)	After digestion (%)	After pH adjustment (%)
Li_2O	18.40	97.35	97.25
B_2O_3	59.4	29.25	25.52
Na_2O	0.87	1.74	1.55
Al_2O_3	1.48	-	-
SiO_2	4.49	1.28	0.95
K_2O	0.31	1.48	0.92
CaO	12.79	1.42	0.52
Fe_2O_3	1.16	0.04	0.01
MgO	0.43	-	-

The dissolution behavior of the constituent elements, presented in Figure 7 and summarized in Table 1, provides a quantitative assessment of solution chemistry and element mobilization efficiency following acid digestion and subsequent pH adjustment. Lithium exhibited an exceptionally high dissolution efficiency of approximately 97-98%, confirming that nearly all lithium initially present in the solid waste is effectively transferred into the aqueous phase, as verified by mass balance calculations based on the initial solid-phase lithium content and the measured leachate concentration. In contrast, boron demonstrated moderate dissolution, with efficiency decreasing from approximately 29% following digestion to ~25% after pH adjustment, attributable to pH-dependent shifts in boron speciation and partial precipitation of borate species at elevated pH values. Other elements - including Si^4, K^+, Ca^{2+}, Fe^{3+}, and Na^+ - exhibited very low dissolution efficiencies (≤2%), with their concentrations declining further upon pH adjustment,

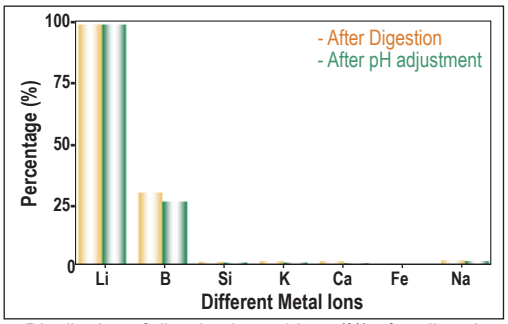


Figure 7. Distribution of dissolved metal ions (%) after digestion and pH adjustment.

indicating predominant retention within the solid residue. Magnesium dissolution was also negligible under the applied conditions, with near-complete retention in the solid phase following pH adjustment. Collectively, these results demonstrate that the digestion protocol enables highly selective lithium mobilization into the aqueous phase while minimizing the co-dissolution of competing elements, yielding a lithium-enriched leachate amenable to subsequent selective adsorption-based recovery.

3.3. Influence of pH and Surface Charge on Lithium Adsorption

Figure 8 illustrates the simultaneous variation of lithium adsorption capacity and zeta potential of HTO as a function of solution pH. The two curves display a clear inverse relationship: as pH increases from 4 to 12, the zeta potential shifts progressively from -16 mV to -63.6 mV, while lithium adsorption capacity increases from ~3 mg·g^{-1} to ~30.6 mg·g^{-1} providing direct mechanistic evidence linking surface deprotonation to enhanced Li^+ uptake [64].

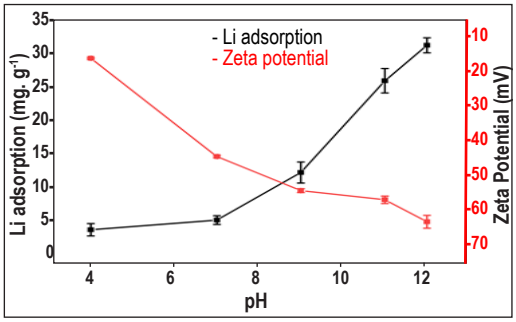


Figure 8. Effect of pH on lithium adsorption capacity and zeta potential of the adsorbent.

At acidic pH (4-7), the low magnitude of the zeta potential reflects the predominance of protonated Ti-OH_2^+ surface species, which reduce the availability of active exchange sites and generate competitive H^+ inhibition of Li^+ insertion into the HTO lattice cavities. Similar pH-dependent suppression of lithium uptake at low pH has been reported for HTO-based ion sieves, where competitive protonation of surface hydroxyl groups is identified as the primary limiting factor [56, 59]. As pH increases beyond 8, progressive deprotonation of Ti-OH groups generates Ti-O^- surface sites that constitute the active Li^+/H^+ exchange positions, and adsorption capacity rises steeply in response. At pH 12, the zeta potential of -63.6 mV confirms a fully deprotonated surface with maximum active site density, consistent with optimal ion-exchange conditions reported for HTO-type materials in the literature [69]. It should be noted that lithium selectivity under these alkaline conditions is governed by the crystallographic cavity size of the HTO framework rather than by electrostatic attraction, as the highly negative surface charge would otherwise favor divalent cations such as Ca^{2+} and Mg^{2+} - an outcome inconsistent with the selectivity results presented in Section 3.9 [70, 71].

Figure 8 illustrates the effect of pH on lithium adsorption capacity onto HTO. As clearly observed, lithium uptake strongly depends on the solution pH. At acidic conditions (pH 4-7), the adsorption capacity remains relatively low, indicating limited interaction between Li^+ ions and the adsorbent surface [56, 63]. This behavior is primarily governed by the surface chemistry of HTO, as evidenced by the characterization results. The FTIR spectra (Figure 6) reveals the presence of abundant surface hydroxyl groups (-OH), which act as active sites for Li^+ adsorption through ion-exchange mechanisms [68, 72].

3.4. Effect of S/L Ratio on Lithium Adsorption

The effect of solid-to-liquid (S/L) ratio on the equilibrium lithium adsorption capacity (q_e) of HTO is presented in Figure 9.

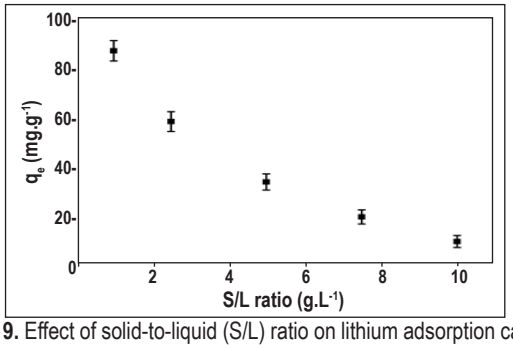


Figure 9. Effect of solid-to-liquid (S/L) ratio on lithium adsorption capacity (q_e).

As the S/L ratio increased from 1 to 10 g/L, q_e decreased monotonically from approximately 36.2 mg·g^{-1} to 15.2 mg·g^{-1}. This inverse relationship between S/L ratio and adsorption capacity is well-established in the ion-sieve literature and can be attributed to two principal factors. First, at lower S/L ratios, the available lithium ions in solution are distributed among fewer adsorbent active sites, resulting in higher site occupancy and consequently higher per-mass adsorption capacity [73]. Second, at elevated S/L ratios, the increased adsorbent loading leads to partial unsaturation of active sites due to the limited availability of Li^+ ions relative to the total number of accessible ion-exchange positions, thereby reducing the experimentally observed q_e [76].

This behavior is consistent with findings reported for analogous titanate ion-sieve systems, where increasing adsorbent dosage has been shown to result in a progressive decline in equilibrium adsorption capacity due to the partial unsaturation of active sites under limited lithium availability [77], and comparable observations have been reported for Al-doped and Zr-doped HTO variants [36, 60, 78]. It is noteworthy that the absence of a distinct inflection point in the present dataset suggests a continuous, gradual transition rather than an abrupt saturation behavior, which may reflect the relatively low initial lithium concentration (200 mg·L^{-1}) employed in this study compared to the highly concentrated brine systems (1000-2000 mg· L^{-1}) typically used in the referenced works - a condition

that inherently limits the driving force for adsorption at higher solid loadings [44, 79]. In the context of practical process design, the S/L ratio of 1 g/L adopted throughout the adsorption studies in this work was selected to maximize the measurable equilibrium capacity under the given concentration conditions, consistent with the experimental approach widely employed in the comparative literature summarized in Table 5 [80]. These results further contextualize the q_e values reported in this study and confirm that the adsorption performance of HTO is strongly dependent on the solid-to-liquid ratio - a parameter that should be explicitly considered when comparing adsorption capacities across different studies.

3.5. Adsorption Isotherms

Figure 10 presents the nonlinear Langmuir and Freundlich isotherm fits for lithium adsorption onto HTO at 298, 308, and 318 K, with the corresponding parameters summarized in Table 2.

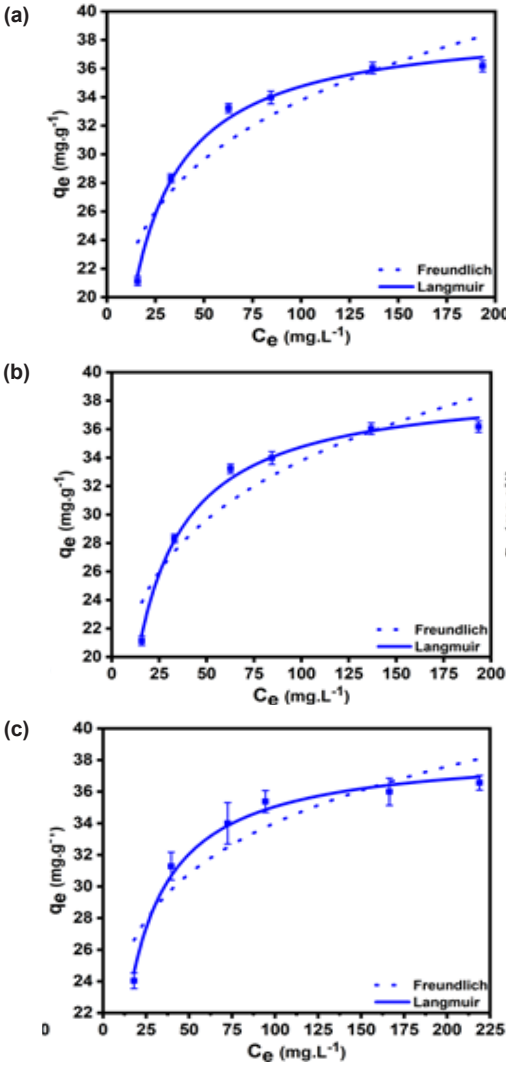


Figure 10. Langmuir and Freundlich isotherm plots for lithium adsorption onto HTO at (a) 298, (b) 308 and (c) 318 K.

The Langmuir model exhibited significantly higher correlation coefficients (R^2 = 0.9986, 0.9934, and 0.9887) than the Freundlich model (R^2 = 0.8441-0.8848), indicating that lithium adsorption is predominantly controlled by monolayer coverage on homogeneous active sites [40, 81]. This behavior is consistent with the ion-sieve mechanism of H_2TiO_3, where Li^+ ions are selectively reinserted into well-defined lattice sites via Li^+/H^+ exchange, inherently satisfying Langmuir assumptions [23, 81]. The Langmuir constant K_L increased from 0.79 to 1.40 L· mg^{-1} with temperature, indicating enhanced binding affinity and stronger interaction between Li^+ and active sites at elevated temperatures. This trend supports the endothermic nature of adsorption and suggests that higher temperatures facilitate Li^+ dehydration and insertion into the titanate structure [70, 82]. The maximum adsorption capacity q_{max} reached 39.27 mg·g^{-1} at 308 K, while experimental values (31.05-36.57 mg·g^{-1}) closely matched model predictions, confirming near-complete occupation of available sites. Although the Freundlich model showed lower fitting accuracy, the parameter n (4.12-6.11) indicates favorable adsorption (n > 1) and relatively uniform adsorption energy distribution [13, 55]. However, the weaker fit confirms that surface heterogeneity plays a secondary role compared to site-specific adsorption. The decrease in K_F with temperature reflects a redistribution of adsorption over a wider concentration range rather than a reduction in overall capacity [83]. The adsorption capacity obtained in this study (23.55 mg·g^{-1} at 308 K), using a leachate derived from XRF melting waste, is comparable to those reported for titanium-based ion sieves, such as 25.80 mg·g^{-1} for geothermal systems [45] and 21.50 mg·g^{-1} for H_2TiO_3 applied to brine solutions [84], highlighting the effectiveness of the synthesized adsorbent.

Table 2. Langmuir and Freundlich isotherm parameters for lithium adsorption at different temperatures

T (K)	q_{max} (mg.g^{-1})	KL (L.mg^{-1})	R^2 (Langmuir)	K_F	n	R^2 (Freundlich)
298	31.13	0.79	0.9986	26.23	4.12	0.8441
308	39.27	0.87	0.9934	17.56	4.43	0.8848
318	38.67	1.40	0.9887	14.15	6.11	0.8528

Overall, the higher correlation coefficients obtained from the Langmuir model (as summarized in Table 2) compared to those from the Freundlich model indicate that Langmuir adsorption dominates the lithium uptake mechanism under the studied conditions. This implies that lithium ions preferentially occupy energetically equivalent adsorption sites on the HTO surface, forming a stable monolayer, while surface heterogeneity plays a secondary role [49, 84].

3.6. Adsorption Thermodynamics

The thermodynamic parameters governing lithium adsorption onto HTO were evaluated using the Van't Hoff approach, and the corresponding ln K° versus 1/T plot is presented in Figure 11.

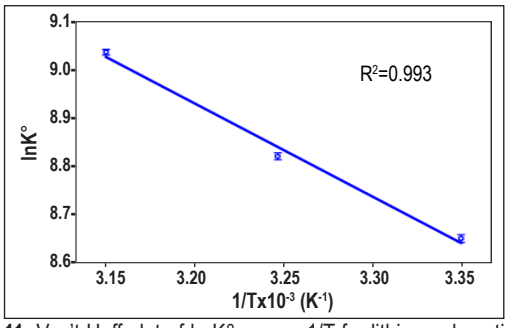


Figure 11. Van't Hoff plot of ln K° versus 1/T for lithium adsorption onto HTO.

The thermodynamic parameters - standard Gibbs free energy change (ΔG°), standard enthalpy change (ΔH°), and standard entropy change (ΔS°) - were derived from the slope and intercept of the linear regression and are summarized in Table 3.

Table 3. The thermodynamic parameters of HTO

T (K)	q_e (mg.g^{-1})	ΔG° (kJ.mol^{-1})	ΔH° (kJ.mol^{-1})	ΔS° (J.mol^{-1}.K^{-1})
298	31.13	0.79	0.9986	26.23
308	39.27	0.87	0.9934	17.56
318	38.67	1.40	0.9887	14.15

The negative ΔG° values obtained at all investigated temperatures (-21.33, -21.79, and -22.37 kJ·mol^{-1} at 298, 308, and 318 K, respectively) confirm that lithium adsorption onto HTO is thermodynamically spontaneous under the applied experimental conditions. The progressive decrease in ΔG° with increasing temperature indicates that the driving force for adsorption becomes stronger at elevated temperatures, implying that the process is thermodynamically more favorable at higher temperatures. This temperature dependence of ΔG° is physically consistent with the endothermic nature of the adsorption process, wherein the entropic contribution to the free energy increasingly offsets the enthalpic cost of adsorption as temperature rises [34]. This finding is consistent with the ion-exchange mechanism of HTO, wherein Li^+ ions replace H^+ ions at crystallographically defined sites within the TiO_6 octahedral framework, a process that inherently involves chemical bond formation and is therefore expected to exhibit chemisorption-like thermodynamic signatures [20].

The positive ΔH° value of +16.44 kJ·mol^{-1} confirms the endothermic nature of lithium adsorption onto HTO. Endothermic adsorption behavior in ion-sieve systems is commonly attributed to the energy required to partially strip the hydration shell surrounding Li^+ ions prior to their insertion into the lattice sites of the adsorbent [44, 68]. In aqueous solution, Li^+ ions are surrounded by a well-organized hydration sphere; the partial desolvation of these ions represents an energy-consuming step that must be overcome before lattice insertion can occur [63, 85]. The relatively modest magnitude of ΔH° (+16.44 kJ·mol^{-1}) suggests that while desolvation is energetically costly, the energy released upon Li^+ insertion into the HTO lattice partially compensates for this cost, resulting in a net endothermic but energetically accessible process [41, 55]. Similar endothermic behavior has been reported for other titanium-based ion-sieve systems; for instance, Chen et al. reported ΔH° = +39.2 kJ·mol^{-1} for a titanium-based ion sieve (PIS-4) applied to geothermal water recovery [45], while Lin et al. reported ΔH° = +8.07 kJ·mol^{-1} for polyporous PVC-HTO composites [86], with the value obtained in the present study falling within this reported range.

The positive ΔS° value of +126.66 J·mol^{-1}·K^{-1} reflects an increase in the degree of disorder at the solid-liquid interface during the adsorption process. This seemingly unexpected result - adsorption typically reduces disorder - can be rationalized by considering that the release of water molecules from the hydration shell of Li^+ ions upon lattice insertion generates a net increase in the freedom of solvent molecules in the bulk solution, thereby increasing the overall entropy of the system [41, 70]. Furthermore, the displacement of H^+ ions from the HTO lattice into the solution phase during the ion-exchange process contributes additional translational degrees of freedom to the liquid phase, further driving the positive entropy change [41]. Positive ΔS° values have been consistently reported for lithium adsorption on ion-sieve materials and are considered a characteristic thermodynamic signature of the H^+/Li^+ exchange mechanism. This trend is well-documented across both manganese- and titanium-based systems; Ding et al. reported ΔS° = +103.51 J·mol^{-1}·K^{-1} for granulated $H_4Mn_5O_{12}$/chitosan composites [85], while Lin et al. reported ΔS° = +46.61 J·mol^{-1}·K^{-1} for polyporous PVC-HTO composites [86]. The ΔS° value of +126.66 J·mol^{-1}·K^{-1} obtained in the present study is higher than both of these reported, which may reflect the comparatively greater degree of solvent reorganization associated with Li^+ insertion into the well-ordered HTO lattice synthesized via the ultrasound-assisted solid-state route, where a higher density of active exchange sites amplifies the cumulative entropic contribution of H^+ displacement into the solution phase.

3.7. Adsorption Kinetics

The kinetic behavior of Li^+ adsorption onto HTO was systematically evaluated using pseudo-first-order (PFO) and pseudo-second-order (PSO) models, as summarized in Table 4 and illustrated in Figure 12a- c. As shown in Figureaa 12a and Table 4, the PFO model yields a poor fit to the experimental data

Table 4. Kinetic parameters for Li^+ adsorption onto HTO obtained from PFO and PSO models

Model	k (rate constant)	q_e (mg.g^{-1})	R^2
Pseudo-first-order	k_1=0.345 h^{-1}	7.59	0.7730
Pseudo-second-order	k_2=0.212 g.mg^{-1}.h^{-1}	37.13	0.9997

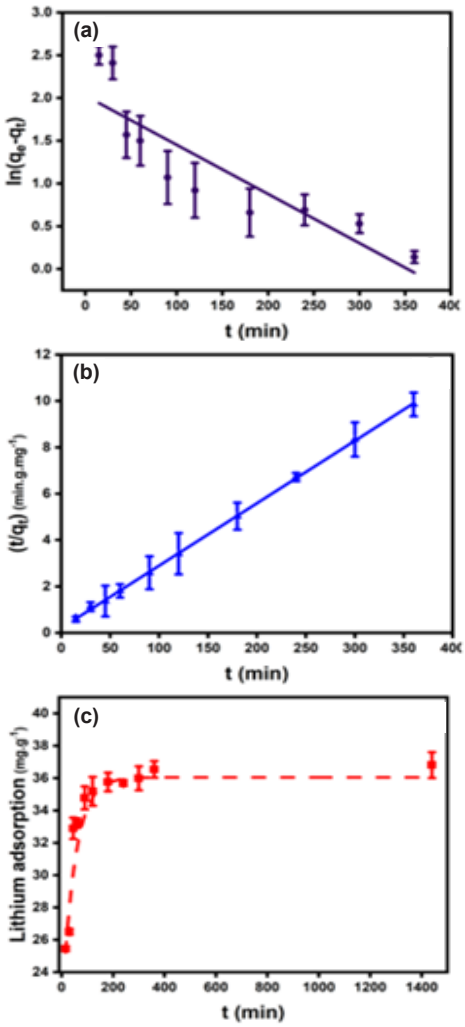


Figure 12. (a) Pseudo-first-order (PFO), (b) pseudo-second-order (PSO) kinetic plots for lithium adsorption onto HTO and (c) lithium adsorption as a function of contact time.

(R^2 = 0.7730), and the calculated equilibrium capacity ($q_{e,cal}$ = 7.59 mg·g^{-1}) deviates dramatically from the experimentally observed value (~36-37 mg·g^{-1}). This discrepancy indicates that the adsorption process is not governed by simple diffusion-controlled physisorption [36]. In contrast, the PSO model provides an excellent description of the kinetic data, as evidenced by the highly linear t/qt versus t relationship in Figure. 12b and the kinetic parameters listed in Table 4 (R^2 = 0.9997 and q_e,cal = 37.13 mg·g^{-1}), which closely matching the experimental value. This finding is consistent with the behavior widely reported for H_2TiO_3-based lithium ion sieves, which conform to PSO kinetics indicative of a chemisorption-controlled mechanism [39, 56]. The relatively high PSO rate constant (k_2 = 0.212 g·mg^{-1}·h^{-1}, Table 4) further indicates rapid surface reaction kinetics, comparable to or exceeding values reported for doped HTO variants in the literature. For reference, Al-doped HTO was reported to achieve an equilibrium capacity of 32.12 mg·g^{-1} under PSO kinetics [60], somewhat lower than the 37.13 mg·g^{-1} obtained in the present work, suggesting competitive adsorption performance of the synthesized material. The overall adsorption profile (Figure 12c) reveals a characteristic two-stage behavior: a rapid initial Li^+ uptake driven by the abundance of accessible surface sites and a high concentration gradient, followed by a gradual approach to equilibrium at approximately 300 min as available sites become progressively occupied. It is worth noting that undoped layered H_2TiO_3 has been reported to require more than 24 h to reach equilibrium [36, 39], making the ~300 min equilibrium time observed here indicative of favorable kinetic characteristics, likely attributable to reduced particle aggregation or enhanced surface accessibility of the synthesized HTO. The dominance of the PSO model is mechanistically consistent with the chemisorption nature of Li^+ uptake on HTO. Although classical Li^+-H^+ ion exchange was long considered the operative mechanism, it has been demonstrated that Li^+ adsorption on HTO proceeds via O-H bond breakage and the formation of O-Li bonds, with isolated hydroxyl groups in the HTi_2 layers playing the primary role [23, 32]. This bond-forming process is inherently second-order in nature, consistent with the PSO behavior observed experimentally [53, 68]. Overall, the kinetic results confirm that Li^+ adsorption onto HTO is predominantly governed by chemisorption at specific surface hydroxyl sites, with the PSO model providing a reliable and physically meaningful description of the process.

3.8. Recycling Experiments

The reusability and structural stability of the adsorbent were systematically evaluated over five successive adsorption-desorption cycles using acidic elution conditions. As illustrated in Figure 13a, the equilibrium lithium adsorption capacity remains nearly unchanged throughout the cycling tests, with only minor fluctuations

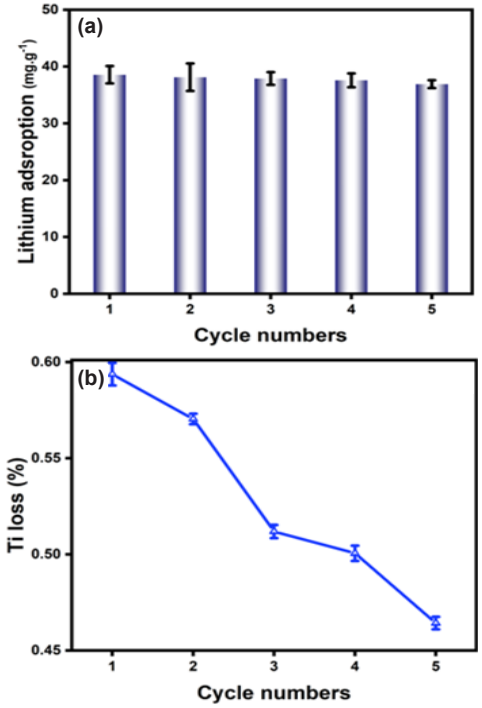


Figure 13. (a) Lithium adsorption capacity retention and (b) titanium loss as a function of cycle number.

observed. This behavior aligns with recent reports on doped-titanium ion sieves, which exhibit capacity retention rates exceeding 95% over multiple cycles, indicating that the active adsorption sites are highly stable and resilient against repeated acid treatment [41].

Simultaneously, Ti loss exhibits a gradual and limited decrease with increasing cycle number, declining from approximately 0.60% in the first cycle to below 0.47% after the fifth cycle (Figure 13b). This value is comparable to, or lower than, the Ti dissolution rates reported for other high-performance adsorbents, such as Co-doped HTO (<0.48%) and PVB-modified HTO (<0.5%), and significantly superior to pristine LTO materials which can suffer higher losses (~1.7-2.6%) [34, 44, 60, 88]. The low extent of Ti leaching, even under acidic elution, suggests that the initial cycles mainly involve the removal of weakly bound surface Ti species, while the bulk crystal framework remains intact [44]. The progressive reduction in Ti loss further implies a stabilization of the adsorbent structure upon repeated cycling.

Importantly, the absence of any noticeable deterioration in lithium adsorption capacity, despite repeated exposure to acidic regeneration, confirms that no significant framework dissolution or structural degradation occurs. These findings provide compelling evidence that the adsorbent maintains its structural integrity and functional performance under harsh regeneration conditions. Overall, the combined stability of lithium uptake and minimal Ti leaching under acid elution conditions highlights the excellent chemical durability and long-term operational robustness of the adsorbent, underscoring its strong potential for practical lithium recovery from industrial effluents and complex aqueous matrices.

Nevertheless, although the adsorbent demonstrates excellent regeneration stability and chemical durability, its powder form may limit direct application in practical systems due to challenges such as solid-liquid separation, potential material loss, and operational constraints. Therefore, for real-world implementation, the material should be transformed into mechanically stable forms such as granules, pellets, or immobilized structures on suitable supports. In this context, while the high regeneration performance highlights the intrinsic potential of the adsorbent, further studies focusing on shaping and process integration are required to enable its practical application [46].

3.9. Adsorption and Selectivity Experiments in Real Sample

The adsorption behavior of different ions on the adsorbent was evaluated in terms of adsorption capacity and separation factor, as illustrated in Figure 14. Among all tested ions, Li^+ exhibited a markedly higher adsorption capacity (~23 $mg.g^{-1}$) compared to competing ions such as K^+, Na^+, Ca^{2+},

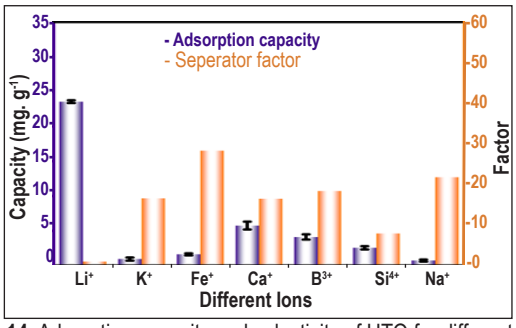


Figure 14. Adsorption capacity and selectivity of HTO for different ions in real melting sample.

Fe^{3+}, B^{3+}, and Si species, whose uptake values remained below 6 $mg.g^{-1}$. This pronounced difference highlights the strong affinity of the adsorbent toward lithium ions which is consistent with previous reports on titanium-based ion sieves where lithium uptake significantly exceeds that of coexisting cations due to the specific ion-memory effect [49]. It should be noted that the comparatively lower lithium adsorption capacity observed in real samples relative to synthetic solutions can be attributed to the higher ionic strength and complex matrix composition of real systems, where competitive ions and dissolved species partially block active sites and reduce the accessibility of lithium to the ion-sieve cavities [89]. Despite the relatively low adsorption capacities observed for the competing ions, their corresponding separation factors were significantly higher than that of Li^+. In particular, Fe, Na, and B ions showed elevated separation factor values, indicating their preferential retention in the aqueous phase rather than on the solid surface [33]. This inverse relationship between adsorption capacity and separation factor further confirms the high selectivity of the adsorbent toward Li^+ ions, as demonstrated in studies where distribution coefficients (K_d) for lithium were found to be orders of magnitude higher than those for interfering ions [57]. Notably, alkali and alkaline earth metals such as K^+, Na^+, and Ca^{2+} -which commonly interfere in lithium recovery from complex brines or industrial waste streams- exhibited minimal adsorption while maintaining high separation factors. This behavior suggests that the adsorption mechanism is not controlled by nonspecific electrostatic interactions but rather by structure-driven or size-selective ion-sieve interactions, favoring Li^+ over larger hydrated ions [32].

Overall, the combined evaluation of adsorption capacity and separation factor demonstrates that the adsorbent possesses excellent lithium selectivity in multi-ion systems, making it a promising candidate for lithium recovery from complex aqueous matrices such as industrial effluents or mineral processing residues [45].

3.10. Adsorption-Desorption Experiments in Real Solution

As shown in Figure 15 Li^+ exhibits a remarkably high desorption efficiency in the real solution, remaining

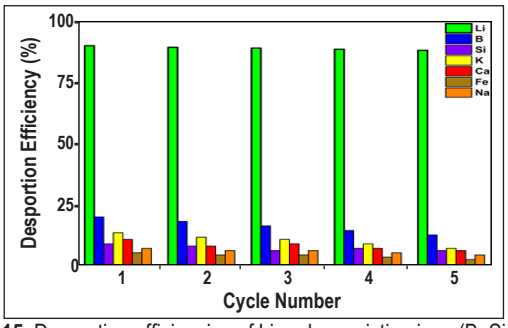


Figure 15. Desorption efficiencies of Li and co-existing ions (B, Si, K, Ca, Fe, and Na) over five consecutive adsorption-desorption cycles.

close to 100% in the first cycle and above ~96% after five consecutive cycles. This behavior indicates excellent regeneration performance and confirms that Li^+ adsorption is highly reversible even in a complex multi-component system. In contrast, co-existing ions such as B, Si, K, Ca, Fe, and Na display significantly lower desorption efficiencies, generally below 20% in the first cycle and decreasing progressively with increasing cycle number. This trend suggests that these ions are either weakly adsorbed (e.g., via physical adhesion on the external surface) [90], or become partially immobilized on the adsorbent surface, resulting in limited reversibility under the applied desorption conditions. Specifically, high-valency cations like Fe^{3+} can form strong, less-reversible complexes with surface hydroxyl groups, while species such as silicates and borates may undergo surface accumulation or polymerization during cyclic pH shifts, leading to their irreversible entrapment and progressive pore blockage [38]. The clear distinction between the desorption behavior of Li^+ and other ions demonstrates that the adsorption-desorption process is predominantly governed by Li^+, confirming the strong selectivity of the synthesized HTO adsorbent under realistic conditions [34]. Furthermore, the stable Li^+ desorption efficiency over repeated cycles highlights the structural robustness and practical applicability of the material for lithium recovery from complex waste-derived solutions.

3.11. Comparison Of The Titanium-Based Lithium-Ion Sieve Developed In This Study With Previously Reported Materials

The selection of a titanium-based ion sieve over manganese-based alternatives was deliberate and mechanistically justified. Manganese-based adsorbents (LMO-type, derived from λ-MnO_2) are frequently cited for their high theoretical adsorption capacities (20-35 mg g^{-1}); however, their practical applicability is fundamentally limited by Mn^{2+} dissolution arising from the Mn^{3+}/Mn^{4+} disproportionation reaction under the acidic elution conditions (typically pH 2-4) required for complete Li^+ desorption [34, 75]. This manganese leaching causes irreversible structural degradation over repeated cycles and introduces metallic contaminants into the lithium product stream - a particularly critical limitation when processing complex waste-derived matrices such as XRF melting leachates, where product purity is paramount [32, 74]. In contrast, the Ti-O bond in HTO-type adsorbents is thermodynamically substantially more stable than the Mn-O bond in spinel structures, rendering titanium-based ion sieves far more resistant to acid-induced dissolution and structural collapse [52, 91]. This inherent chemical durability is reflected in the cycling stability observed in the present study, where the adsorbent maintained consistent lithium uptake over five successive adsorption-desorption cycles with Ti leaching declining progressively from ~0.60% to below 0.47% - confirming that the bulk Ti-O framework remains structurally intact under repeated acidic regeneration.

As presented in Table 5, the adsorption performance of titanium-based lithium-ion sieves varies significantly depending on synthesis method, particle

Table 5. Comparisons of different HTO on lithium adsorption performance.

Synthesis method	Particle size (nm)	BET ($m^2.g^{-1}$)	Solution	Li concentration ($mg.L^{-1}$)	pH	Li adsorption ($mg.g^{-1}$)	Adsorption time (h)	Cycle number	Refs
Sol-Gel	60-80	-	LiOH	2000	12	24.6	22	-	[83]
Hydrothermal	50-70	-	LiCl	118	9.1	39.43	120	-	[92]
	100-200	-	Brine	1560	8.8	32.8	3	6	[95]
Solid phase reaction	100-300	22.3	LiOH	2000	12	27.8	8	6	[50]
	100	58.94	LiOH	280	12	28	1.5	-	[88]
	100-300	18.2	LiOH	70	11.5	33.6	24	5	[93]
	100-200	18	LiCl	1000	10	32.2	0.5	-	[94]
	50-150	36	LiCl	1000	12	28	0.5	-	[94]
	50-1200	-	Brine	1950	10.1	16.68	3	3	[48]
	100-200	-	Brine	1630	6.7	32.6	24	-	[49]
	70	-	Brine	669	10.1	24.5	12	5	[54]
	100-200	-	Brine	15600	8.8	34.8	24	9	[76]
Solid phase reaction (Ultrasonic assisted)	-	18.6	LiCl	200	12	36.18	6	5	This work
	-	18.6	XRF Waste	1040	12	23.55	6	5	This work

characteristics, and solution composition. In synthetic solutions, several HTO materials exhibit relatively high lithium adsorption capacities (≈28-39 mg g^{-1}), although this is often achieved under high lithium concentrations and strongly alkaline conditions, and in some cases with prolonged equilibrium times (up to 120 h). In contrast, studies conducted with real brine solutions generally report lower adsorption capacities (≈16-34 mg g^{-1}), reflecting the complexity of multicomponent systems and competitive ion effects. Moreover, adsorption kinetics in brine systems vary widely, with equilibrium times ranging from a few hours to over 24h.

In this context, the HTO adsorbent synthesized in this study via an ultrasonic-assisted solid-state route demonstrates a competitive adsorption capacity (36.18 mg.g^{-1}) under moderate conditions (LiCl, 200 mg L^{-1}, pH 12), while achieving equilibrium within a relatively short time (~6 h). More importantly, when applied to real XRF waste solution (1040 mg L^{-1} Li), the adsorbent maintains a considerable adsorption capacity (23.55 mg.g^{-1}) with similar kinetics, confirming its effectiveness in complex matrices. These results indicate that the developed material offers a balanced combination of adsorption capacity, kinetics, and stability, and demonstrates its practical applicability for lithium recovery from both synthetic and real waste-derived solutions.

4. Conclusion

This study demonstrates the feasibility of lithium recovery from XRF melting waste using a titanium-based ion-sieve adsorbent synthesized via a solid-state route. The protonation of Li_2TiO_3 successfully produced H_2TiO_3 (HTO) with enhanced surface area (18.6 $m^2.g^{-1}$) and preserved structural integrity, which are critical for ion-sieving performance. The applied acid digestion process enabled highly selective lithium dissolution, achieving approximately 97-98% lithium transfer into the aqueous phase, while minimizing the co-dissolution of competing elements.

Adsorption experiments revealed a strong pH dependence, with optimal performance observed under alkaline conditions (pH 12). The maximum adsorption capacity reached 36.18 mg.g^{-1} at 308 K in synthetic solutions, while a capacity of 23.55 mg.g^{-1} was obtained for real XRF-derived leachate, confirming the applicability of the adsorbent in complex multi-component systems. Isotherm analysis indicated that lithium adsorption follows the Langmuir model (R^2 ≈0.99), suggesting monolayer adsorption on homogeneous active sites, with a maximum theoretical capacity of 39.27 mg g^{-1}. Kinetic studies demonstrated that the process is well described by the pseudo-second-order model (R^2 = 0.9997), indicating a chemisorption-controlled mechanism. Thermodynamic parameters (ΔG° ≈-21 to -22 kJ mol^{-1}, ΔH° = +16.44 kJ·mol^{-1}) confirmed that the adsorption is spontaneous and endothermic.

Importantly, the adsorbent exhibited excellent stability, maintaining nearly constant adsorption capacity over five cycles, with titanium loss decreasing from ~0.60% to below 0.47%, demonstrating strong structural robustness under acidic regeneration conditions.

When compared with previously reported titanium-based ion-sieve materials (Table 5), the adsorption capacity obtained in this study (36.18 mg.g^{-1}) falls within the upper range of values reported for solid-state synthesized HTO (≈28-39 mg g^{-1}), while offering a relatively short equilibrium time (~6 h) compared to many literature studies requiring up to 24-120 h. Furthermore, the performance achieved in real waste-derived solution (23.55 mg.g^{-1}) is comparable to or higher than several reported values for complex brine systems (≈16-34 mg.g^{-1}), highlighting the effectiveness of the developed material under realistic conditions.

Overall, this work not only introduces a novel application of titanium-based ion sieves for lithium recovery from XRF melting waste but also demonstrates competitive adsorption performance, favorable kinetics, and excellent stability compared to existing materials. These findings confirm the strong potential of H_2TiO_3 for lithium recovery from unconventional secondary resources and contribute to the development of sustainable, circular-economy-based lithium supply strategies.

5. Acknowledgement

The authors would like to thank TENMAK-Boron Research Institute for providing the research infrastructure and laboratory facilities that enabled this study.

6. Author Contribution Statement

Sezgin Özkasapoğlu: Conceptualization, methodology, execution of the synthesis, primary investigation, data collection, writing-original draft preparation and formal analysis of all characterization data

Hüseyin Çelikkan: Supervision, writing-review and editing.

7. Conflict of Interest

Authors have no conflict of interest.

References

[1] Ryu, T., Shin, J., Ghoreishian, S. M., Chung, K.-S., & Huh, Y. S. (2019). Recovery of lithium in seawater using a titanium intercalated lithium manganese oxide composite. *Hydrometallurgy*, *184*, 22-28. https://doi.org/10.1016/j.hydromet.2018.12.012

[2] Guo, X., Zhang, J., & Tian, Q. (2021). Modeling the potential impact of future lithium recycling on lithium demand in China: A dynamic SFA approach. *Renewable and Sustainable Energy Reviews*, *137*, 110461. https://doi.org/10.1016/j.rser.2020.110461

[3] Boroumand, Y., & Razmjou, A. (2024). Adsorption-type aluminium-based direct lithium extraction: The effect of heat, salinity and lithium content. *Desalination*, *577*, 117406. https://doi.org/10.1016/j.desal.2024.117406

[4] Kavanagh, L., Keohane, J., Garcia Cabellos, G., Lloyd, A., & Cleary, J. (2018). Global lithium sources-industrial use and future in the electric vehicle industry: A review. *Resources*, *7*(3), 57. https://doi.org/10.3390/resources7030057

[5] Gardiner, N. J., Jowitt, S. M., & Sykes, J. P. (2024). Lithium: Critical, or not so critical? *Geoenergy*, *2*(1), geoenergy2023-2045. https://doi.org/10.1144/geoenergy2023-045

[6] Szlugaj, J., & Radwanek-Bąk, B. (2022). Lithium sources and their current use. *Gospodarka Surowcami Mineralnymi*, *38*(1), 61-88. https://doi.org/10.24425/gsm.2022.140613

[7] Zhang, J., Cheng, Z., Qin, X., Gao, X., Wang, M., & Xiang, X. (2023). Recent advances in lithium extraction from salt lake brine using coupled and tandem technologies. *Desalination*, *547*, 116225. https://doi.org/10.1016/j.desal.2022.116225

[8] Alessia, A., Alessandro, B., Maria, V.-G., Carlos, V.-A., & Francesca, B. (2021). Challenges for sustainable lithium supply: A critical review. *Journal of Cleaner Production*, *300*, 126954. https://doi.org/10.1016/j.jclepro.2021.126954

[9] Marcinov, V., Klimko, J., Takáčová, Z., Piroškova, J., Miškufová, A., Sommerfeld, M., … & Oráč, D. (2023). Lithium production and recovery methods: Overview of lithium losses. *Metals*, *13*(7), 1213. https://doi.org/10.3390/met13071213

[10] Meng, F., McNeice, J., Zadeh, S. S., & Ghahreman, A. (2021). Review of lithium production and recovery from minerals, brines, and lithium-ion batteries. *Mineral Processing and Extractive Metallurgy Review*, *42*(2), 123-141. https://doi.org/10.1080/08827508.2019.1668387

[11] Raiguel, S., Nguyen, V. T., Reis Rodrigues, I., Deferm, C., Riaño, S., & Binnemans, K. (2023). Recovery of lithium from simulated nanofiltration-treated seawater desalination brine using solvent extraction and selective precipitation. *Solvent Extraction and Ion Exchange*, *41*(4), 425-448. https://doi.org/10.1080/07366299.2023.2206440

[12] Wesselborg, T., Virolainen, S., & Sainio, T. (2021). Recovery of lithium from leach solutions of battery waste using direct solvent extraction with TBP and FeCl3. *Hydrometallurgy*, *202*, 105593. https://doi.org/10.1016/j.hydromet.2021.105593

[13] Nampeera, J. (2021). *Functionalized cellulose-based adsorbent for lithium recovery from aqueous solutions* [Master's thesis, İzmir Institute of Technology]. İzmir, Türkiye

[14] Zhang, Y.-n., Yu, D.-h., Jia, C.-y., Sun, L.-y., Tong, A., Wang, Y., … & Tang, J.-g. (2023). Advances and promotion strategies of membrane-based methods for extracting lithium from brine. *Desalination*, *566*, 116891. https://doi.org/10.1016/j.desal.2023.116891

[15] Lu, M., Miao, Y., Yang, Y., & Li, P. (2024). Continuous recovery of lithium and boron from Jezechake Salt Lake brine using fixed-bed adsorbers. *Hydrometallurgy*, *226*, 106299. https://doi.org/10.1016/j.hydromet.2024.106299

[16] Park, S. H., Kim, J. H., Moon, S. J., Jung, J. T., Wang, H. H., Ali, A., … & Lee, Y. M. (2020). Lithium recovery from artificial brine using energy-efficient membrane distillation and nanofiltration. *Journal of Membrane Science*, *598*, 117683. https://doi.org/10.1016/j.memsci.2019.117683

[17] Li, Y., Wang, M., Xiang, X., Zhao, Y., & Peng, Z. (2023). Separation performance and fouling analyses of nanofiltration membrane for lithium extraction from salt lake brine. *Journal of Water Process Engineering*, *54*, 104009. https://doi.org/10.1016/j.jwpe.2023.104009

[18] Li, Z., Li, C., Liu, X., Cao, L., Li, P., Wei, R., … & Lai, Z. (2021). Continuous electrical pumping membrane process for seawater lithium mining. *Energy & Environmental Science*, *14*(5), 3152-3159. https://doi.org/10.1039/D1EE00354B

[19] Wang, J., Yue, X., Wang, P., Yu, T., Du, X., Hao, X., … & Guan, G. (2022). Electrochemical technologies for lithium recovery from liquid resources: A review. *Renewable and Sustainable Energy Reviews*, *154*, 111813. https://doi.org/10.1016/j.rser.2021.111813

[20] Kahvecioglu, A. (2022). *Adsorbent Synthesis For The Recovery of Lithium From Water Resources* [Master's thesis, İzmir Institute of Technology]. İzmir.

[21] Sun, J., Li, X., Huang, Y., Luo, G., Tao, D., Yu, J., Chen, L., Chao, Y., & Zhu, W. (2023). Preparation of high hydrophilic H2TiO3 ion sieve for lithium recovery from liquid lithium resources. *Chemical Engineering Journal*, *453*, 139485. https://doi.org/10.1016/j.cej.2022.139485

[22] Nikfar, S., Fahimi, A., & Vahidi, E. (2025). Unlocking sustainable lithium: A comparative life cycle assessment of innovative extraction methods from brine. *Resources, Conservation and Recycling*, *212*, 107977. https://doi.org/10.1016/j.resconrec.2024.107977

[23] Lu, M., Miao, Y., Yang, Y., & Li, P. (2024). DFT calculation and experiments for Li+/H+ ion-exchange on titanium-based lithium ion-sieves. *Chemical Engineering Science*, *300*, 120619. https://doi.org/10.1016/j.ces.2024.120619

[24] Orooji, Y., Nezafat, Z., Nasrollahzadeh, M., Shafiei, N., Afsari, M., Pakzad, K., & Razmjou, A. (2022). Recent advances in nanomaterial development for lithium ion-sieving technologies. *Desalination*, *529*, 115624. https://doi.org/10.1016/j.desal.2022.115624

[25] Chang, S. A., & Balouch, A. (2024). Analytical perspective of lithium extraction from brine waste: Analysis and current progress. *Microchemical Journal*, *200*, 110291. https://doi.org/10.1016/j.microc.2024.110291

[26] Mends, E. A., & Chu, P. (2023). Lithium extraction from unconventional aqueous resources-a review on recent technological development for seawater and geothermal brines. *Journal of Environmental Chemical Engineering*, *11*(5), 110710. https://doi.org/10.1016/j.jece.2023.110710

[27] Xiong, J., Zhao, Z., Liu, D., & He, L. (2022). Direct lithium extraction from raw brine by chemical redox method with LiFePO4/FePO4 materials. *Separation and Purification Technology*, *290*, 120789. https://doi.org/10.1016/j.seppur.2022.120789

[28] Liu, G., Zhao, Z., & Ghahreman, A. (2019). Novel

approaches for lithium extraction from salt-lake brines: A review. *Hydrometallurgy*, *187*, 81-100. https://doi.org/10.1016/j.hydromet.2019.05.005

[29] Recepoğlu, Y. K., Kabay, N., Yoshizuka, K., Nishihama, S., Yılmaz-Ipek, İ., Arda, M., & Yüksel, M. (2018). Effect of operational conditions on separation of lithium from geothermal water by λ-MnO2 using ion exchange-membrane filtration hybrid process. *Solvent Extraction and Ion Exchange*, *36*(5), 499-512. https://doi.org/10.1080/07366299.2018.1529232

[30] Recepoğlu, Y. K. (2025). Optimized Lithium (I) Recovery from Geothermal Brine of Germencik, Türkiye, Utilizing an Aminomethyl phosphonic Acid Chelating Resin. *Solvent Extraction and Ion Exchange*, *43*(1), 23-44. https://doi.org/10.1080/07366299.2024.2404146

[31] Recepoğlu, Y. K., & Özşen, A. Y. (2025). Hydrometallurgy of lithium: Selective separation from geothermal brines using chitosan-lithium ion sieve composite. *Turkish Journal of Analytical Chemistry*, *7*(2), 140-153. https://doi.org/10.51435/turkjac.1629713

[32] Chen, Q., Chen, Z., Li, H., & Ni, B.-J. (2024). Advanced lithium ion-sieves for sustainable lithium recovery from brines. *Sustainable Horizons*, *9*, 100093. https://doi.org/10.1016/j.horiz.2024.100093

[33] Wang, S., Zhang, M., Zhang, Y., Zhang, Y., Qiao, S., & Zheng, S. (2019). Application of citric acid as eluting medium for titanium type lithium ion sieve. *Hydrometallurgy*, *183*, 166-174. https://doi.org/10.1016/j.hydromet.2018.12.002

[34] Zhao, K., Li, J., Yuan, J., Yu, X., Guo, Y., Jiang, Z., Li, M., Duo, J., & Deng, T. (2024). A novel Co-doped H2TiO3 spinning composite for efficient lithium recovery from alkaline lithium precipitation mother liquor. *Chemical Engineering Journal*, *482*, 148989. https://doi.org/10.1016/j.cej.2024.148989

[35] Farahbakhsh, J., Arshadi, F., Mofidi, Z., Mohseni-Dargah, M., Kök, C., Assefi, M., … & Boroumand, Y. (2024). Direct lithium extraction: A new paradigm for lithium production and resource utilization. *Desalination*, *575*, 117249. https://doi.org/10.1016/j.desal.2023.117249

[36] Pu, X., Du, X., Jing, P., Wei, Y., Wang, G., Xian, C., … & Ji, X. (2021). Interface and defect engineering enable fast and high-efficiency Li extraction of metatitanic acid adsorbent. *Chemical Engineering Journal*, *425*, 130550. https://doi.org/10.1016/j.cej.2021.130550

[37] Hartikainen, S. (2026). *3D-printed lithium-ion-sieve adsorbents for lithium recovery from Li-ion battery metals recycling process raffinates* [Master's thesis, Lappeenranta-Lahti University of Technology LUT]. Lappeenranta, Finland.

[38] Yu, J., Zhu, J., Luo, G., Chen, L., Li, X., Cui, P., Wu, P., Chao, Y., Zhu, W., & Liu, Z. (2023). 3D-printed titanium-based ionic sieve monolithic adsorbent for selective lithium recovery from salt lakes. *Desalination*, *560*, 116651. https://doi.org/10.1016/j.desal.2023.116651

[39] Zhang, P., Yang, M., Xu, C., Wang, Q., He, C., Liu, C., & Lai, B. (2024). Insight into the synergistic mechanism of Co and N doped titanium-based adsorbents for liquid lithium extraction. *Chemical Engineering Journal*, *480*, 147631. https://doi.org/10.1016/j.cej.2023.147631

[40] Zhang, G., Wei, Q., Xia, X., Huang, D., Tang, W., & Yu, W. W. (2025). Synergistic doping and coating of lithium ion-sieves for enhanced lithium recovery from brine. *Desalination*, *601*, 118556. https://doi.org/10.1016/j.desal.2025.118556

[41] Zhang, H., Dong, B., Yang, Y., Long, X., Chen, H., Pan, J., & Zhou, C. Cu-Doped Titanium Lithium-Ion Sieves with Improved Hydrophilicity for Efficient Extraction of Lithium from Aqueous Resources. *Available at SSRN 4805268*. https://doi.org/10.1016/j.cej.2024.153545

[42] Liu, Q., Xing, H., Zhang, Y., Zhao, Y., Rong, M., Liu, H., & Yang, L. (2024). Highly hydrophilic H2TiO3 ion sieve with neodymium (Nd) doping enables fast and high-efficiency Li extraction. *Separation and Purification Technology*, *345*, 127263. https://doi.org/10.1016/j.seppur.2024.127263

[43] Wang, S., Zhang, M., Zhang, Y., Zhang, Y., Qiao, S., & Zheng, S. (2019). High adsorption performance of the Mo-doped titanium oxide sieve for lithium ions. *Hydrometallurgy*, *187*, 30-37. https://doi.org/10.1016/j.hydromet.2019.05.004

[44] Lawagon, C. P., Nisola, G. M., Mun, J., Tron, A., Torrejos, R. E. C., Seo, J. G., Kim, H., & Chung, W.-J. (2016). Adsorptive Li+ mining from liquid resources by H2TiO3: Equilibrium, kinetics, thermodynamics, and mechanisms. *Journal of Industrial and Engineering Chemistry*, *35*, 347-356. https://doi.org/10.1016/j.jiec.2016.01.015

[45] Chen, S., Chen, Z., Wei, Z., Hu, J., Guo, Y., & Deng, T. (2021). Titanium-based ion sieve with enhanced post-separation ability for high performance lithium recovery from geothermal water. *Chemical Engineering Journal, 410*, 128320. https://doi.org/10.1016/j.cej.2020.128320

[46] Zhang, L., He, G., Zhou, D., Zhou, J., & Yao, Q. (2016). Study on transformation mechanism of lithium titanate modified with hydrochloric acid. *Ionics*, *22*, 2007-2014. https://doi.org/10.1007/s11581-016-1742-x

[47] Sujoto, V. S. H., Prasetya, A., Sutijan, Astuti, W., Jenie, S. N. A., Anggara, F., & Murti Petrus, H. T. B. (2026). Development and optimisation of titanium-based lithium-ion sieves through solid-state synthesis for high-efficiency *Brine lithium recovery. Transition Metal Chemistry*, *51*(4). https://doi.org/10.1007/s11243-025-00693-z

[48] Ji, Z.-Y., Yang, F.-J., Zhao, Y.-Y., Liu, J., Wang, N., & Yuan, J.-S. (2017). Preparation of titanium-base lithium ionic sieve with sodium persulfate as eluent and its performance. *Chemical Engineering Journal*, *328*, 768-775. https://doi.org/10.1016/j.cej.2017.07.047

[49] Chitrakar, R., Makita, Y., Ooi, K., & Sonoda, A. (2014). Lithium recovery from salt lake brine by H2TiO3. *Dalton Transactions*, *43*, 8933-8939. https://doi.org/10.1039/C4DT00467A

[50] Tang, D., Zhou, D., Zhou, J., Zhang, P., Zhang, L., & Xia, Y. (2015). Preparation of H2TiO3-lithium adsorbent using low-grade titanium slag. *Hydrometallurgy*, *157*, 90-96. https://doi.org/10.1016/j.hydromet.2015.07.009

[51] Qu, W., Fu, Y., Zhang, Y., Wang, W., Xu, C., Liu, C., … & Liu, B. (2024). Structural/surficial dual regulated granular H2TiO3 lithium-ion sieves for lithium extraction from salt lake brine. *Journal of Cleaner Production*, *449*, 141789. https://doi.org/10.1016/j.jclepro.2024.141789

[52] Xu, X., Zhou, Y., Fan, M., Lv, Z., Tang, Y., Sun, Y., … & Wan, P. (2017). Lithium adsorption performance of a

three-dimensional porous H2TiO3-type lithium ion-sieve in strong alkaline Bayer liquor. *RSC Advances*, *7*(31), 18883-18891. https://doi.org/10.1039/C7RA01056G

[53] Marthi, R., Yang, P., Owusu-Fordjour, E., & Smith, Y. (2022). Role of stacking faults and hydroxyl groups on the lithium adsorption/desorption properties of layered H2TiO3. *Materials Today Advances*, *14*, 100237. https://doi.org/10.1016/j.mtadv.2022.100237

[54] Gu, D., Sun, W., Han, G., Cui, Q., & Wang, H. (2018). Lithium ion sieve synthesized via an improved solid state method and adsorption performance for West Taijinar Salt Lake brine. *Chemical Engineering Journal*, *350*, 474-483. https://doi.org/10.1016/j.cej.2018.05.191

[55] Wang, S., Li, P., Cui, W., Zhang, H., Wang, H., Zheng, S., & Zhang, Y. (2016). Hydrothermal synthesis of lithium-enriched β-Li2TiO3 with an ion-sieve application: Excellent lithium adsorption. *RSC Advances*, *6*, 102608-102616. https://doi.org/10.1039/C6RA18018C

[56] Xiao, X., Li, J., Qiu, K., Chen, M., & Zhang, X. (2024). Dual surfactants-assisted adsorption of lithium ions in liquid lithium resources on a superhydrophilic spinel-type H4Ti5O12 ion sieve. *Separation and Purification Technology*, *330*, 125479. https://doi.org/10.1016/j.seppur.2023.125479

[57] Zhang, Q., Hai, C., Sun, Y., Gao, Y., Dong, S., … & Zhou, Y. (2025). Formation and working mechanisms of layered TiO2.H2O adsorbents for effectively recovering Li+ from oil-gas field brines. *Separation and Purification Technology*, *354*, 128998. https://doi.org/10.1016/j.seppur.2024.128998

[58] Li, Y., Yang, Z., & Ma, P. (2023). Research progress on new types of H2TiO3 lithium-ion sieves: A review. *Metals*, *13*(5), 977. https://doi.org/10.3390/met13050977

[59] Wu, M., Wang, S., Jiang, M., Lei, Z., Xiong, S., & Chu, J. (2025). Preparation of W-doped titanium lithium ion sieve by hydrothermal method and enhanced adsorption performance for Li+. *Ionics, 31*, 3421-3432. https://doi.org/10.1007/s11581-025-06104-8

[60] Dai, X., Zhan, H., Qian, Z., Li, J., Liu, Z., & Wu, Z. (2021). Al-doped H2TiO3 ion sieve with enhanced Li+ adsorption performance. *RSC Advances*, *11*, 34988-34995. https://doi.org/10.1039/D1RA06535A

[61] Wang, Y., Xie, Y., Guo, X., Yan, X., Chen, Y., Hu, P., … & Lang, W. (2026). Morphological convergence in solid-state synthesis: Unveiling the critical role of TiO2 precursor size for high-performance H2TiO3 lithium ion-sieves. *Particuology*, *110*, 1-13. https://doi.org/10.1039/10.1016/j.partic.2025.12.023

[62] Xu, J., Wei, X., Han, J., & Qin, W. (2024). Synthesis and optimisation mechanism of functionalised adsorption materials for lithium-ion extraction from salt water: A review. *Separation and Purification Technology*, *339*, 126237. https://doi.org/10.1016/j.seppur.2023.126237

[63] Zhao, B., Li, J., Zhang, M., Qiao, Y., Feng, S., & Liu, Z. (2026). Interfacial mechanism and kinetic characteristics of lithium adsorption on spinel titanium nanoplates. *Colloids and Surfaces A: Physicochemical and Engineering Aspects*, *736*, 139676. https://doi.org/10.1016/j.colsurfa.2026.139676

[64] Wu, J., Wang, W., Chen, W., Liu, C., Deng, T., & Yu, X. (2025). Inorganic porous carbon as the supporter of H2TiO3 via in-situ polymerization synchronous conversion for lithium recovery from aqueous solutions. *Separation and Purification Technology*, *356*, 129806. https://doi.org/10.1016/j.seppur.2024.129806

[65] Qian, H., Huang, S., Ba, Z., Wang, W., Yu, F., Liang, D., … & Wang, Y. (2021). HTO/cellulose aerogel for rapid and highly selective Li+ recovery from seawater. *Molecules*, *26*(13), 4054. https://doi.org/10.3390/molecules26134054

[66] Li, N., Gan, K., Lu, D., Zhang, J., & Wang, L. (2018). Preparation of three-dimensional macroporous-mesoporous lithium ion sieve with high Li+ adsorption capacity. *Research on Chemical Intermediates*, *44*, 1105-1117. https://doi.org/10.1007/s11164-017-3154-6

[67] Wang, Q., Yang, X., Li, C., Zhao, C., Huang, Y., Qiu, S., Qin, Y., & Shi, C. (2024). Titanium-based lithium ion sieve adsorbent H2TiO3 with enhanced Li+ adsorption properties by magnetic Fe doping. *Separation and Purification Technology, 346*, 127455. https://doi.org/10.1016/j.seppur.2024.127455

[68] Marthi, R., Asgar, H., Gadikota, G., & Smith, Y. R. (2021). On the structure and lithium adsorption mechanism of layered H2TiO3. *ACS Applied Materials & Interfaces*, *13*(7), 8361-8369. https://doi.org/10.1021/acsami.0c20691

[69] Ding, Y., Nhung, N. T. H., An, J., Chen, H., Liao, L., He, C., … & Fujita, T. (2023). Manganese-titanium mixed ion sieves for the selective adsorption of lithium ions from an artificial salt lake brine. *Materials*, *16*(11), 4190. https://doi.org/10.3390/ma16114190

[70] Li, X., Cheng, H., Li, G., Chen, Z., Yu, H., Zheng, J., … & Tian, Z. (2026). Lattice anchoring via Ni doping empowers a robust H2TiO3 adsorbent for lithium extraction in strongly alkaline solutions. *Chemical Engineering Journal*, *172979*. 10.1016/j.cej.2026.172979

[71] He, G., Zhang, L., Zhou, D., Zou, Y., & Wang, F. (2015). The optimal condition for H2TiO3-lithium adsorbent preparation and Li+ adsorption confirmed by an orthogonal test design. *Ionics*, *21*, 2219-2226. https://doi.org/10.1007/s11581-015-1393-3

[72] Safari, S., Lottermoser, B. G., & Alessi, D. S. (2020). Metal oxide sorbents for the sustainable recovery of lithium from unconventional resources. *Applied Materials Today*, *19*, 100638. https://doi.org/10.1016/j.apmt.2020.100638

[73] Tian, L., Ma, W., & Han, M. (2010). Adsorption behavior of Li+ onto nano-lithium ion sieve from hybrid magnesium/lithium manganese oxide. *Chemical Engineering Journal*, *156*(1), 134-140. https://doi.org/10.1016/j.cej.2009.10.008

[74] Wang, S., Chen, X., Zhang, Y., Zhang, Y., & Zheng, S. (2018). Lithium adsorption from brine by iron-doped titanium lithium ion sieves. *Particuology*, *41*, 40-47. https://doi.org/10.1016/j.partic.2018.02.001

[75] İpek, O. (2024). *Lithium recovery from water by granulated pvc pan-titanium type lithium Ion-sieve* [Master's thesis, Izmir Institute of Technology]. İzmir, Türkiye.

[76] Shen, Z., Qi, S., Hong, C., Wang, X., Han, Z., Chen, J., Wu, Y., Han, T., Gu, J., & Xu, L. (2025). Preparation of zirconium-doped titanium ion sieve composites and lithium adsorption from salt-lake brine. *Desalination*, *602*, 118618. https://doi.org/10.1016/j.desal.2025.118618

[77] Nyarangi, C., Nunna, P. R. T., Abu-Zahra, N., Baig, N., Abdulazeez, I., & Aljundi, I. H. (2023). Optimizing the synthesis process for Lithium-Ion sieve adsorbents: Effect of calcination temperature and heating rate on reaction efficiency and performance. *Materials & Design*, *235*, 112417. https://doi.org/10.1016/j.matdes.2023.112417

[78] Ma, T., Jin, Z., Jia, Z., & Peng, W. (2025). Synthesis of doped titanium-based lithium adsorbents with excellent stability and adsorption performance by solid state reactions. *Desalination*, *594*, 118300. https://doi.org/10.1016/j.desal.2024.118300

[79] Zhang, G., Hai, C., Zhou, Y., Zhang, J., Liu, Y., Zeng, J., … & Wu, Z. (2023). Synthesis and performance estimation of a granulated PVC/PAN-lithium ion-sieve for Li+ recovery from brine. *Separation and Purification Technology*, *305*, 122431. https://doi.org/10.1016/j.seppur.2022.122431

[80] Wei, S., Wei, Y., Chen, T., Liu, C., & Tang, Y. (2020). Porous lithium ion sieves nanofibers: General synthesis strategy and highly selective recovery of lithium from brine water. *Chemical Engineering Journal*, *379*, 122407. https://doi.org/10.1016/j.cej.2019.122407

[81] Zhang, L., Zhou, D., Yao, Q., & Zhou, J. (2016). Preparation of H2TiO3-lithium adsorbent by the sol-gel process and its adsorption performance. *Applied Surface Science*, *368*, 82-87. https://doi.org/10.1016/j.apsusc.2016.01.203

[82] Wang, X., Jiang, X., Wu, J., Zhao, K., Guo, Y., Deng, T., & Yu, X. (2023). Recovery of lithium from brine with different degrees of mineralization by resorcinol/urea-formaldehyde foam-supported H2TiO3. *Chemical Engineering Journal*, *462*, 142285. https://doi.org/10.1016/j.cej.2023.142285

[83] Li, X., Chao, Y., Chen, L., Chen, W., Luo, J., Wang, C., … & Zhu, W. (2020). Taming wettability of lithium ion sieve via different TiO2 precursors for effective Li recovery from aqueous lithium resources. *Chemical Engineering Journal*, *392*, 123731. https://doi.org/10.1016/j.cej.2019.123731

[84] Lin, H., Yu, X., Li, M., Duo, J., Guo, Y., & Deng, T. (2019). Synthesis of polyporous ion-sieve and its application for selective recovery of lithium from geothermal water. *ACS Applied Materials & Interfaces*, *11*(29), 26364-26372. https://doi.org/10.1021/acsami.9b07401

[85] Ding, W., Zhang, J., Liu, Y., Guo, Y., Deng, T., & Yu, X. (2021). Synthesis of granulated H4Mn5O12/chitosan with improved stability by a novel cross-linking strategy for lithium adsorption from aqueous solutions. *Chemical Engineering Journal*, *426*, 131689. https://doi.org/10.1016/j.cej.2021.131689

[86] Zhang, Y., Liu, J., Yang, Y., Lin, S., & Li, P. (2021). Preparation of granular titanium-type lithium-ion sieves and recyclability assessment for lithium recovery from brines with different pH value. *Separation and Purification Technology*, *267*, 118613. https://doi.org/10.1016/j.seppur.2021.118613

[87] Knapik, E., Rotko, G., Marszałek, M., & Piotrowski, M. (2023). Comparative study on lithium recovery with ion-selective adsorbents and extractants: Results of multi-stage screening test with the use of brine simulated solutions with increasing complexity. *Energies*, *16*(7), 3149. https://doi.org/10.3390/en16073149

[88] Luo, G., Li, X., Chen, L., Chao, Y., & Zhu, W. (2023). Electrochemical lithium ion pumps for lithium recovery: A systematic review and influencing factors analysis. *Desalination*, *548*, 116228. https://doi.org/10.1016/j.desal.2022.116228

[89] Reich, R., Slunitschek, K., Danisi, R. M., Eiche, E., & Kolb, J. (2023). Lithium extraction techniques and the application potential of different sorbents for lithium recovery from brines. *Mineral Processing and Extractive Metallurgy Review*, *44*(4), 261-280. https://doi.org/10.1080/08827508.2022.2047041

[90] Zhang, T., Liu, Y., Peng, Y., & Qiu, F. (2024). In situ carbonized cellulose-based hybrid aerogels for lithium adsorption and recovery. *Biomass Conversion and Biorefinery, 14*, 7139-7147. https://doi.org/10.1007/s13399-022-03199-1

[91] Ye, S., Yang, C., Sun, Y., Guo, C., Wang, J., Chen, Y., … & Qiu, T. (2024). Application and mechanism of lithium-ion sieves in the recovery of lithium-containing wastewater: A review. *Water, Air, & Soil Pollution*, *235*, 272. https://doi.org/10.1007/s11270-024-07085-6

[92] Moazeni, M., Hajipour, H., Askari, M., & Nusheh, M. (2015). Hydrothermal synthesis and characterization of titanium dioxide nanotubes as novel lithium adsorbents. *Materials Research Bulletin, 61*, 70-75. https://doi.org/10.1016/j.materresbull.2014.09.069

[93] Loganathan, P., Naidu, G., & Vigneswaran, S. (2017). Mining valuable minerals from seawater: a critical review. *Environmental Science: Water Research & Technology, 3*, 37-53. https://doi.org/10.1039/C6EW00268D

[94] Hayashi, F., Ogawa, K., Moriya, Y., Sudare, T., & Teshima, K. (2018). Growth of β-Li2TiO3 nanocrystals from LiCl and LiOH fluxes. *Crystal Growth & Design*, *19*(2), 1377-1383. https://doi.org/10.1021/acs.cgd.8b01758

[95] Wang, S., Li, P., Zhang, X., Zheng, S., & Zhang, Y. (2017). Selective adsorption of lithium from high Mg-containing brines using HXTiO3 ion sieve. *Hydrometallurgy*, *174*, 21-28. https://doi.org/10.1016/j.hydromet.2017.09.009